

# Single-Component Molecular Metals with Extended-TTF Dithiolate Ligands

Akiko Kobayashi,<sup>\*,†</sup> Emiko Fujiwara,<sup>†</sup> and Hayao Kobayashi<sup>‡</sup>

Research Centre for Spectrochemistry, Graduate School of Science, The University of Tokyo, Hongo, Bunkyo-ku, Tokyo 113-0033, Japan; and  
Institute for Molecular Science, Myodaiji, Okazaki, Aichi 444-8585, Japan

Received March 8, 2004

## Contents

1. Introduction	5243
2. Frontier Orbital Engineering in Molecular Systems	5245
2.1. Design of $\pi$ Metal Band	5245
2.2. Design of Molecule with Small HOMO–LUMO Gap	5246
2.3. Molecular Design of a Metallic Crystal Based on Intramolecular Electron Transfer between HOMO and LUMO Bands	5247
2.4. Syntheses of Metal Dithiolate Complexes with Extended-TTF Ligands	5247
2.4.1. Cross-Coupling Reaction	5248
2.4.2. Pseudo-Wittig Reaction	5248
2.4.3. Syntheses of Neutral Metal Complexes	5249
2.5. The First Single-Component Molecular Metal, [Ni(tmdt) <sub>2</sub> ]	5249
2.6. Analogous Single-Component Molecular Metals	5253
3. Development of New Functional Single-Component Molecular Conductors with Extended-TTF Dithiolate Ligands	5256
3.1. Single-Component Paramagnetic Conductor [Cu(dmdt) <sub>2</sub> ]	5256
3.2. Metallic Crystal of [Co(dt) <sub>2</sub> ] <sub>2</sub> with a Dimeric Conformation	5257
3.3. Single-Component Antiferromagnetic Molecular Metal, [Au(tmdt) <sub>2</sub> ], with $T_N$ around 100 K	5258
3.4. Single-Component Pd Complexes	5260
4. Infrared Electronic Absorption in Single-Component Molecular Metals	5261
5. Conclusions and Future Prospects	5263
6. Acknowledgments	5263
7. References	5263

## 1. Introduction

About three decades ago, the existence of metal electrons in molecular crystals was proved by X-ray (or neutron) experiments on Peierls instability (or giant Kohn anomaly) of a partially oxidized platinum complex, K<sub>2</sub>[Pt(CN)<sub>4</sub>Br<sub>0.3</sub>]<sub>2</sub>·3H<sub>2</sub>O (KCP salt), with a one-dimensional (1D) Pt chain structure.<sup>1,2</sup> Though high-pressure investigation of KCP salt suggested the possibility of suppression of Peierls transition above

70 kbar,<sup>3</sup> the insulating instability was considered to be an inherent character of the molecular metal system because the existence of molecular metals was verified by the observation of the metal instability. Almost at the same time, (TTF)(TCNQ) (TTF = tetrathiafulvalene; TCNQ = tetracyanoquinodimethane; for structures, see Chart 1) with a metallic state down to about 55 K was discovered.<sup>4</sup> These findings aroused much interest of physicists and chemists and opened a new era of low-dimensional molecular metals. From the chemical viewpoint, these conductors provided a new challenging problem on the design and development of molecular conductors without metal instabilities. It may be said that the recent development of organic conductors is based mostly on the design of two-dimensional (2D) electronic states by the introduction of sulfur or selenium atoms to  $\pi$  electron systems. The origin of the two-dimensionality of the system can be interpreted on the basis of the simple extended-Hückel tight-binding band examinations, which provided a guiding principle for the design of new molecular conductors. Besides molecular conductors based on multi-sulfur  $\pi$ -donor molecules, development of the molecular conductors based on multi-sulfur  $\pi$ -acceptor molecules was also performed based on molecular designing analysis using band structure calculations. Needless to say, the first organic superconductor (TMTSF)<sub>2</sub>PF<sub>6</sub> (TMTSF = tetramethyltetraselenafulvalene) was discovered in 1980, which was most important in the history of organic conductors.<sup>5</sup> The famous general phase diagram of a series of TMTSF conductors including analogous TMTTF (= tetramethyltetrathiafulvalene) systems was presented around 1990.<sup>6</sup> Examination of its crystal structures and extended-Hückel tight-binding electronic band structure calculations of this system provided an important guideline for the design of 2D molecular metals and superconductors.<sup>7</sup> In (TMTSF)<sub>2</sub>PF<sub>6</sub>, close intermolecular Se···Se contacts were observed between the TMTSF stacks.<sup>8</sup> From a structural–chemical point of view, (TMTSF)<sub>2</sub>PF<sub>6</sub> was the first molecular conductor in which we clearly noticed the existence of organic conductors with 2D conduction pathways though the band structure calculation gave a warped quasi-1D Fermi surface. From then on, extensive efforts have been devoted to developing new types of molecular metals and superconductors by enhancing interstack interactions. The ideally 2D organic metals with a superconducting ground state

\* To whom correspondence should be addressed. E-mail: akiko@chem.s.u-tokyo.ac.jp.

<sup>†</sup> The University of Tokyo.

<sup>‡</sup> Institute for Molecular Science, Myodaiji. E-mail: hayao@ims.ac.jp.



Akiko Kobayashi was born in 1943 in Tokyo, Japan. She studied Chemistry at the University of Tokyo and obtained a doctor's degree in 1972. She became a Research Associate at the University of Tokyo in 1972 and was promoted to an Associate Professor at the Department of Chemistry in 1993, and in 1999 she took up a position as a Professor at the Research Centre for Spectrochemistry, Graduate School of Science, the University of Tokyo. She studied molecular conductors such as 1D platinum complexes, BEDT-TTF,  $M(\text{dmit})_2$ , DCNQI, and BETS systems and recently single-component molecular metals. Her present main interests are in the development of new molecular systems, such as single-component molecular metals.



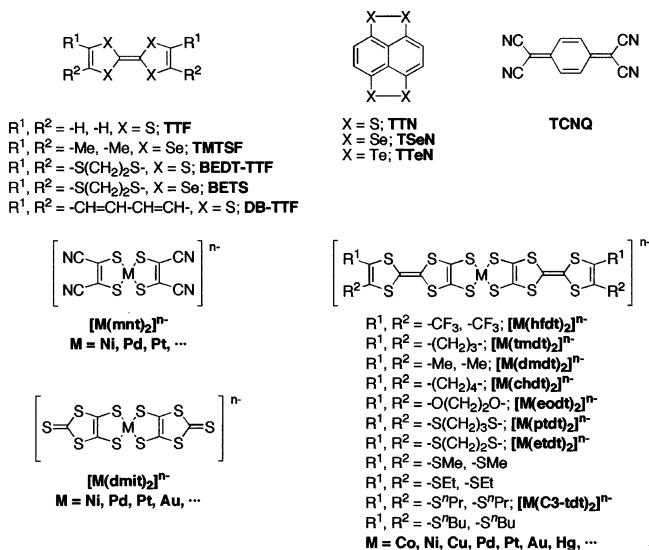
Emiko Fujiwara was born in 1972 in Miyagi, Japan. She studied Chemistry and received her Ph.D. degree from the Graduate University for Advanced Studies in 2000. After a postdoctoral position at National Institute of Advanced Industrial Science and Technology (2000–2001) and a JSPS postdoctoral fellowship in the laboratory of Professor Akiko Kobayashi (2001–2002), she was appointed a Research Associate at the University of Tokyo in 2003. Her research interests include material chemistry and structural chemistry of molecular conductors, especially multifunctional molecular systems including magnetic properties.

were confirmed by the first discoveries of the  $\beta$ - and especially  $\kappa$ -type BEDT-TTF superconductors (BEDT-TTF = bis(ethylenedithio)tetrathiafulvalene).<sup>9–11</sup> Another conductor which gave us an important hint was a platinum dithiolate complex,  $(\text{H}_3\text{O})_x\text{Li}_y[\text{Pt}(\text{mnt})_2] \cdot z\text{H}_2\text{O}$ , exhibiting a metal–insulator (MI) transition around 220 K [mnt = 1,2-dicyano-1,2-ethylenedithiolato (maleonitriledithiolate)], where intermolecular  $\text{S} \cdots \text{S}$  contacts were found to be essential to form a conduction band similar to the case of organic conductors based on TTF-like  $\pi$  donor molecules.<sup>12</sup> The first molecular superconductor based on transition metal complexes is (TTF)[Ni(dmit)<sub>2</sub>]<sub>2</sub>, developed by Cassoux et al. in 1986 (dmit = 4,5-dimercapto-1,3-dithiole-2-thion).<sup>13</sup> [M(dmit)<sub>2</sub>] (M = Ni, Pd) superconductors occupy a unique position because almost all molecular superconductors were systems com-



posed of organic  $\pi$  donor molecules having TTF-like skeletons. Although [Ni(dmit)<sub>2</sub>]<sub>2</sub><sup>14</sup> resembles the BEDT-TTF molecule, the transverse interactions were found to be weaker than expected and were not sufficient for the realization of the 2D molecular interaction.<sup>14</sup> X-ray diffuse scattering experiments and the band structure calculations including both the LUMO (the lowest unoccupied molecular orbital) and the HOMO (the highest occupied molecular orbital) bands of the [Ni(dmit)<sub>2</sub>] acceptor molecules suggested the existence of the multi-Fermi surfaces in the TTF[Ni(dmit)<sub>2</sub>]<sub>2</sub> system.<sup>15</sup> In addition to the conventional conductors based on  $\pi$  donor (or acceptor) molecules and closed-shell inorganic counteranions (or cations), magnetic organic conductors such as paramagnetic organic superconductors,<sup>16</sup> antiferromagnetic organic superconductors,<sup>17</sup> and ferromagnetic metals,<sup>18</sup> consisting of  $\pi$  donors and magnetic anions, have been recently developed.

### Chart 1



posed of organic  $\pi$  donor molecules having TTF-like skeletons. Although [Ni(dmit)<sub>2</sub>]<sub>2</sub><sup>14</sup> resembles the BEDT-TTF molecule, the transverse interactions were found to be weaker than expected and were not sufficient for the realization of the 2D molecular interaction.<sup>14</sup> X-ray diffuse scattering experiments and the band structure calculations including both the LUMO (the lowest unoccupied molecular orbital) and the HOMO (the highest occupied molecular orbital) bands of the [Ni(dmit)<sub>2</sub>] acceptor molecules suggested the existence of the multi-Fermi surfaces in the TTF[Ni(dmit)<sub>2</sub>]<sub>2</sub> system.<sup>15</sup> In addition to the conventional conductors based on  $\pi$  donor (or acceptor) molecules and closed-shell inorganic counteranions (or cations), magnetic organic conductors such as paramagnetic organic superconductors,<sup>16</sup> antiferromagnetic organic superconductors,<sup>17</sup> and ferromagnetic metals,<sup>18</sup> consisting of  $\pi$  donors and magnetic anions, have been recently developed.

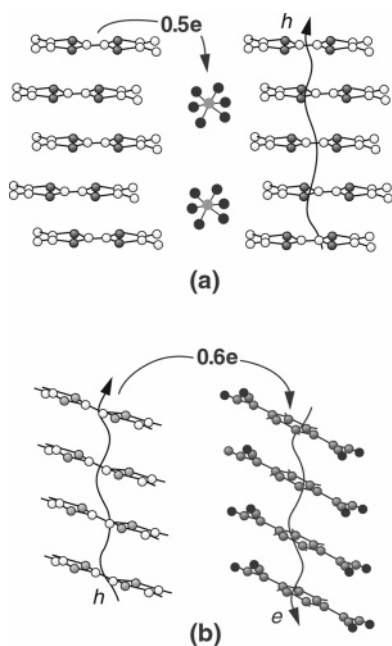


**Figure 1.** Schematic picture illustrating two essential requirements to design molecular metals: (1) the formation of electronic bands and (2) the generation of charge carriers. (a) TMTSF molecule forms a conduction band, and metal electrons are generated by electron transfer between TMTSF and PF<sub>6</sub><sup>-</sup> anions. (b) In the case of (TTF)(TCNQ), free carriers are generated in both columns by partial charge transfer between TTF and TCNQ.

Thus, an extremely large amount of progress has been made in the field of molecular crystals in the last quarter century. However, a difficult problem has remained unsolved. The realization of a molecular metal based on single-component molecules had been one of the important targets in the field of molecular conductors since the discovery of semiconducting properties of organic materials around 1950.<sup>19,20</sup> In contrast to typical inorganic metals composed of single elements, such as sodium and copper, all of the molecular metals developed until recently had consisted of more than two components. It has been believed for a long time that the formation of electronic bands and the generation of charge carriers by the intermolecular charge transfer between the molecules constituting the band (designated by A) and other chemical species (designated by B) are two essential requirements to design molecular metals. In some cases, both molecules A and B form conduction bands where the electron and the hole carriers are generated on both A and B molecules. This is the reason the design of metals composed of single-component molecules is difficult. Needless to say, in the first organic superconductor (TMTSF)<sub>2</sub>PF<sub>6</sub>, TMTSF molecules form a conduction band and metal electrons are produced by electron transfer between TMTSF and PF<sub>6</sub><sup>-</sup> [(TMTSF<sup>+0.5</sup>)<sub>2</sub>(PF<sub>6</sub><sup>-</sup>)] (Figure 1a). In the case of (TTF)(TCNQ) with segregated columns of TTF and TCNQ, free carriers are generated in both columns by partial charge transfer between TTF and TCNQ (TTF<sup>+0.6</sup>TCNQ<sup>-0.6</sup>) (Figure 1b). Similar carrier generation processes are also required in conducting organic polymers (e.g. chemical doping of polyacetylene<sup>21</sup>). The difficulty in designing a single-component molecular metal is naturally related to the facts

that molecules usually have an even number of electrons and that the highest occupied molecular orbital is doubly occupied. There are trials to develop highly conducting systems by using stable organic radical molecules with singly occupied molecular orbitals.<sup>22</sup> However, these molecules tend to produce narrow half-filled bands, where electrons will be localized by correlation even when the electronic band is formed. Thus, the molecular crystal consisting of single-component molecules was long believed to be an insulator because of the absence of the carriers.<sup>23</sup>

However, we have recently noticed the possibility of carrier generation even in the single-component molecular crystal and prepared the first example of the crystal of a neutral transition metal complex with extended-TTF ligands, [Ni(tmdt)<sub>2</sub>] (tmdt = trimethylenetetrafulvalenedithiolate), exhibiting metallic behavior down to very low temperature.<sup>24,25</sup> More recently, direct experimental evidence for the Fermi surface in [Ni(tmdt)<sub>2</sub>] was obtained by detecting the quantum oscillations in magnetization at very high magnetic field (or the de Haas–van Alphen (dHvA) effect).<sup>26</sup> Torque magnetometry measurements of single crystals of [Ni(tmdt)<sub>2</sub>] using a sensitive micro-cantilever at low temperature revealed dHvA oscillatory signals for all directions of a magnetic field, showing the presence of three-dimensional (3D) electron and hole Fermi surfaces. Thus, the existence of a single-component molecular metal has been definitely confirmed.

This review will describe the frontier orbital engineering for the design of a single-component molecular metal first and then will present some examples of recently developed single-component molecular conductors with various extended-TTF ligands.

## 2. Frontier Orbital Engineering in Molecular Systems

The molecule is a nanosized functional unit and the frontier orbital engineering is a starting point in the bottom-up construction of molecular systems with desired electronic functions. In this section, the design of  $\pi$  molecular metals is discussed on the basis of a simple extended-Hückel tight-binding band picture. Here, a  $\pi$  molecular metal stands for a metal composed of molecules with the frontier orbitals HOMO and/or LUMO with a “ $\pi$  character”.

### 2.1. Design of $\pi$ Metal Band

As mentioned above, the “partial charge transfer” between the electronic band derived from the HOMO (or LUMO) and other chemical species had been believed to be inevitable to generate the carriers in the molecular crystal, and this was the reason all the molecular metals developed before 2000 are composed of more than two components. However, we have recently noticed that the carrier generation will become possible by the “electron transfer between HOMO and LUMO bands” even in a “neutral single-component molecular crystal” if we can develop a molecule with a very small HOMO–LUMO gap and sufficiently large intermolecular interactions (especially transverse intermolecular interactions). As previously reported,<sup>25</sup> in order to realize such a

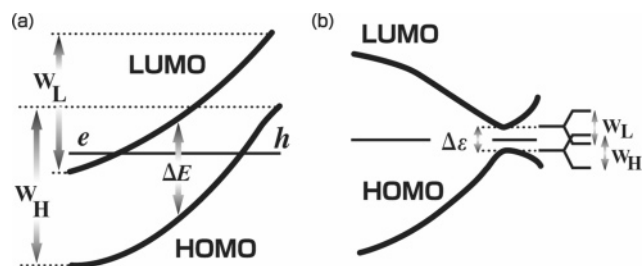


**Figure 2.** Schematic drawing of band structure (see text): (a) parallel band; (b) crossing band.  $W_H$  and  $W_L$  show the bandwidths of the HOMO band and the LUMO band, respectively.  $\Delta E$  is the HOMO–LUMO energy separation.  $\Delta\epsilon$  is an energy gap produced by the HOMO–LUMO interaction. The transverse bandwidths  $W_H$  and  $W_L$  are produced by transverse HOMO–HOMO and LUMO–LUMO interactions.

“electron transfer”, the energy difference between the HOMO and LUMO ( $\Delta E$ ) must be small compared with the bandwidth ( $\Delta E < (W_H + W_L)/2$ , where  $W_H$  and  $W_L$  are the widths of the HOMO and the LUMO bands, respectively) (Figure 2a). Since the bandwidth in an ordinary organic metal is about 0.5–1.0 eV,  $\Delta E$  must be less than 0.5 eV ( $\approx 4000 \text{ cm}^{-1}$ ), which means that a very anomalous molecule with electronic excitation energy (or HOMO–LUMO gap) in the infrared energy region must be developed in order to meet this condition. In the following discussion, we assume that the condition  $\Delta E < (W_H + W_L)/2$  is satisfied. Since the symmetry of the HOMO is different from that of the LUMO, the sign of the intermolecular overlap integral ( $S$ ) (or the transfer integral ( $t = kS$ ;  $k \approx -10 \text{ eV}$ )) of the HOMO–HOMO interaction ( $S_{HH}$ ) is apt to be different from that of the LUMO–LUMO interaction ( $S_{LL}$ ). This situation is serious especially in highly 1D conductors with “crossing bands” of HOMO and LUMO (see Figure 2b), because in this case the HOMO–LUMO interaction ( $t_{HL}$ ) destroys Fermi surfaces. Since the HOMO of the TTF-like  $\pi$  donor has the same sign on every sulfur (or selenium) atom (Figure 3a),  $S_{HH}$  has a negative sign along the molecular stacking direction (that is, the direction of the largest interaction) in an ordinary conducting system. However,  $S_{LL}$  tends to have an opposite sign due to the “intermolecular slipping configuration” frequently found in crystals of molecular conductors where the neighboring molecule is displaced along the long axis of the molecule. This is the reason the crossing bands tend to be realized. One way to protect the Fermi surface from HOMO–LUMO interaction ( $t_{HL}$ ) is the enhancement of transverse interactions, which is almost the same condition required to stabilize the metallic state of the molecular conductor against 1D metal instability. If the energy gap ( $\Delta\epsilon$ ) produced by the HOMO–LUMO interaction is less than the bandwidth in the transverse direction ( $w_H, w_L$ ) ( $\Delta\epsilon < w_H, w_L$ ), it is highly possible that the electron and hole carriers are generated and the system becomes (semi-)metallic.<sup>25</sup> Thus, in usual molecular conductors, the enhancement of 2D intermolecular interactions (that is,  $w_H$  and  $w_L$ ) is essential.

On the other hand, if we can realize a molecular arrangement where  $S_{HH}$  and  $S_{LL}$  have the same sign, the system has “parallel bands”. Then the Fermi

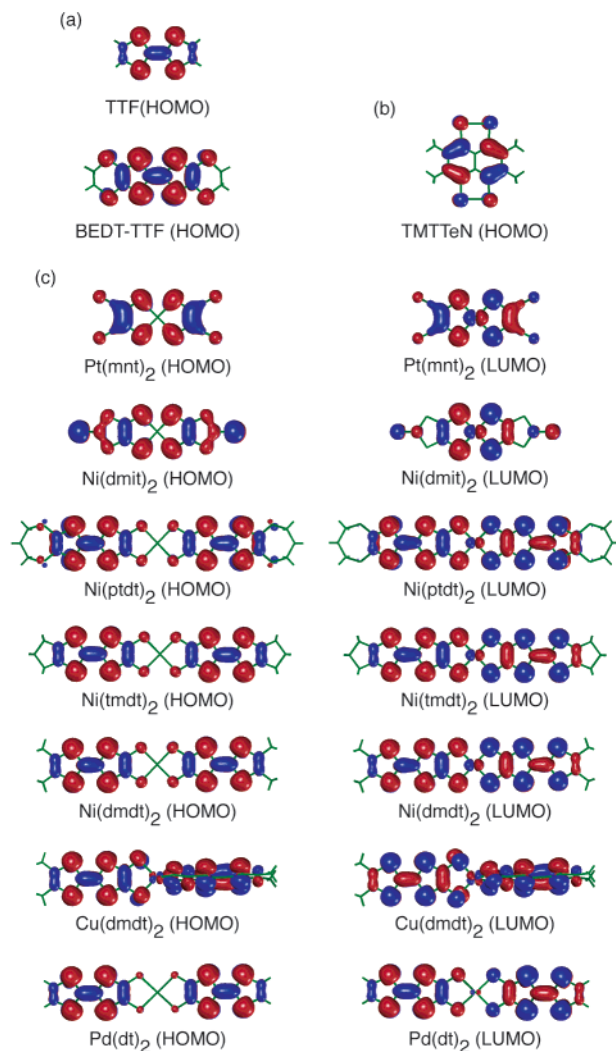


**Figure 3.** Schematic drawing of (a) the HOMO of a TTF-like  $\pi$  donor molecule, (b) the LUMO of a TMTTeN molecule, and (c) the HOMO and LUMO of metal dithiolate complexes, [Pt(mnt)<sub>2</sub>] and [Ni(dmit)<sub>2</sub>], and metal dithiolate complexes with extended-TTF ligands, [Ni(ptdt)<sub>2</sub>], [Ni(tmdt)<sub>2</sub>], [Ni(dmdt)<sub>2</sub>], [Cu(dmdt)<sub>2</sub>], and [Pd(dt)<sub>2</sub>].

surfaces are stable for the HOMO–LUMO interaction (see Figure 2a). If the adjacent molecule slips along the short-axis of the molecule,  $S_{LL}$  becomes negative in the same way as  $S_{HH}$ . Then, the system has parallel bands and large Fermi surfaces will be derived from HOMO and LUMO bands.

We have recently found that Canadell et al. has discussed independently the possibility of the existence of similar molecular metals by using “internal electron transfer” in the two-band systems.<sup>27</sup>

## 2.2. Design of Molecule with Small HOMO–LUMO Gap

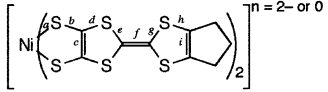
As mentioned above, if the energy of the top of the HOMO band is higher than that of the bottom of the LUMO band, the electrons and holes will be generated by the electron transfer between these two bands. But this special situation will be possible only when the HOMO–LUMO gap ( $\Delta E$ ) is anomalously small. To develop the metal system consisting of single-component molecules, we must prepare a very unusual molecule with (1) extremely small  $\Delta E$  and

(2) sufficiently large intermolecular interactions (especially transverse interactions). To satisfy these two conditions simultaneously, we adopted the transition metal dithiolate complexes with extended-TTF ligands. Since the HOMO and LUMO of a metal dithiolate complex can be roughly considered to be constructed from bonding and antibonding combinations of left and right ligand orbitals (except the small contribution of the d orbital of the central transition metal atom), the HOMO–LUMO separation ( $\Delta E$ ) will tend to be small with increasing size of the extended-TTF ligand system. An indication of a very small HOMO–LUMO gap of this type of molecule was first suggested by *ab initio* MO calculation of  $[\text{Ni}(\text{ptdt})_2]$  (ptdt = propylenedithiotetrathiafulvalenedithiolate).<sup>28</sup> In addition, to obtain the large intermolecular transverse interactions, it is very important to utilize the molecule with TTF-like structure because the HOMO of the TTF-like donor has the same sign on every sulfur atom. In this case, all the intermolecular contacts through sulfur atoms can contribute additively to enhance the intermolecular interaction. Therefore, the realization of close transverse intermolecular contacts in these systems will mean the realization of large transverse intermolecular interactions. However, this is not always true in other organic conductors composed of different multi-sulfur  $\pi$  donor molecules. For example, in the case of the well-known  $\pi$  donors TTN (or TSN) (= tetrathionaphthacene), TSeN (= tetraselena-naphthacene), and TTeN (= tetratelluronaphthacene) with peripheral chalcogen atoms, the HOMO has a node on the chalcogen–chalcogen bond, which tends to cancel transverse HOMO–HOMO interactions through chalcogen atoms (Figure 3b).<sup>29</sup>

### 2.3. Molecular Design of a Metallic Crystal Based on Intramolecular Electron Transfer between HOMO and LUMO Bands

As mentioned above, the HOMO and LUMO of a metal dithiolate complex with extended-TTF ligands can be roughly written as  $\phi_H = \phi_1 + \phi_2$  and  $\phi_L = \phi_1 - \phi_2 + c_M\phi_{d\pi}$ , where  $\phi_1$  and  $\phi_2$  represent the left half and the right half of the ligand wave function and  $c_M\phi_{d\pi}$  is the small contribution from the  $d\pi$  orbital of the central metal atom. Unlike  $\phi_H$ ,  $\phi_L$  can be mixed with the  $d\pi$  orbital of the central metal atom. To obtain a more precise picture of the symmetries and the energy levels of the HOMO and LUMO of metal complexes with TTF-like ligands, *ab initio* MO calculations were performed on a  $[\text{Ni}(\text{ptdt})_2]$  molecule.<sup>28</sup> The calculation of the singlet ground state of  $[\text{Ni}(\text{ptdt})_2]$  based on the optimized molecular structure, which has a good planarity and has approximately a  $D_{2h}$  symmetry except for the propylenedithio group, showed the symmetries of  $b_{2g}$  for the HOMO and  $b_{1u}$  for the LUMO, which are similar to those of the dmit metal complexes. The schematic drawings of the HOMO and LUMO orbitals are shown in Figure 3c, and their respective symmetries are consistent with the above discussion. Comparison of the results of calculations performed on the lowest triplet state and the singlet state suggests that the energy difference between the HOMO and LUMO is very small. To

**Table 1. Average Bond Lengths (Å) of the Dianion ( $n = 2-$ ) and Neutral ( $n = 0$ )  $[\text{Ni}(\text{tmdt})_2]^n$**



bond	$n = 2-$	$n = 0$	$\Delta$
<i>a</i>	2.2034(5)	2.177(1)	-26
<i>b</i>	1.742(2)	1.717(3)	-25
<i>c</i>	1.339(4)	1.352(6)	13
<i>d</i>	1.767(2)	1.750(3)	-17
<i>e</i>	1.760(2)	1.742(3)	-18
<i>f</i>	1.344(4)	1.360(5)	16
<i>g</i>	1.772(2)	1.751(3)	-21
<i>h</i>	1.744(2)	1.731(3)	3
<i>i</i>	1.340(4)	1.333(6)	-7

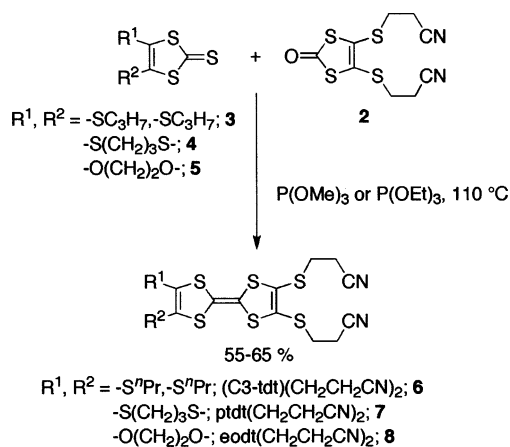
obtain experimental evidence for the validity of this simple idea for the orbital design of a  $\pi$  molecule with a very small HOMO–LUMO gap, we compared the bond lengths of dianionic and corresponding neutral dithiolate complex molecules determined by X-ray structure analyses. Table 1 shows the data for the bond lengths of  $[\text{Ni}(\text{tmdt})_2]$  dianionic and neutral molecules, which suggested the bonding nature of the LUMO on C=C bonds and the antibonding nature on C–S bonds, as expected from the frontier orbitals shown in Figure 3c.<sup>30</sup> Similar results were also obtained in the  $[\text{Cu}(\text{dmdt})_2]$  system (see section 3.1).<sup>31</sup>

On the basis of these analyses, we could derive the newly revised requirements for the design of molecular metals, including single-component molecular metal systems: (1) band formation by realizing a suitable arrangement of the molecules with suitable frontier molecular orbitals and (2) carrier generation by the intermolecular charge transfer between the molecules constituting the conduction band and other chemical species or by intramolecular electron transfer between HOMO and LUMO bands of the same molecule.

### 2.4. Syntheses of Metal Dithiolate Complexes with Extended-TTF Ligands

Before describing the first single-component molecular metal, we briefly mention syntheses of various metal dithiolate complexes with extended-TTF ligands. Several strategies can be used to prepare asymmetrically bis-protected TTFs. The synthesis of such structurally modified TTFs can be divided roughly into two different synthetic methods. Namely, (i) the most common method is the trialkyl phosphite mediated cross-coupling reaction<sup>32</sup> between appropriate chalcogenons, and (ii) the other one is pseudo-Wittig condensation<sup>33</sup> leading to the desired species. Roughly speaking, the former and latter are applicable to the syntheses of the TTFs substituted with alkylthio or alkyloxy groups and alkyl groups, respectively. 4,5-Bis(2'-cyanoethylthio)-1,3-dithiole-2-thione (**1**) and 4,5-bis(2'-cyanoethylthio)-1,3-dithiol-2-one<sup>34</sup> (**2**) were selected as the key compounds for the synthesis of asymmetrically bis-protected TTFs, because the TTFs substituted with two polar cyanoethyl groups have an advantage of an easy separation from byproducts using column chromatography.

Scheme 1



## 2.4.1. Cross-Coupling Reaction

The mechanism proposed in the literature<sup>35,36</sup> suggests a thiophilic addition of trialkyl phosphite on the chalcogen atom localized on the 2-position of the chalcogenone. A subsequent elimination of a chalcogeno phosphite finally leads to the TTF skeleton. According to the difference of the substituents on the 4,5-positions, the degree of the thiophilic addition by trialkyl phosphite is determined. Synthesis of the dithiolate ligand moieties with the alkylthio or alkyloxy groups and the cyanoethyl-protecting groups was performed according to the reported method by Becher et al.<sup>37,38</sup> The thiophilic addition of trialkyl phosphite occurs easily for the 1,3-dithiole-2-chalcogenone with the alkylthio or alkyloxy substituents on the 4,5-positions, while it is difficult to obtain the TTFs substituted with the alkyl groups on the 4,5-positions by such a trialkyl phosphite-mediated cross-coupling reaction.

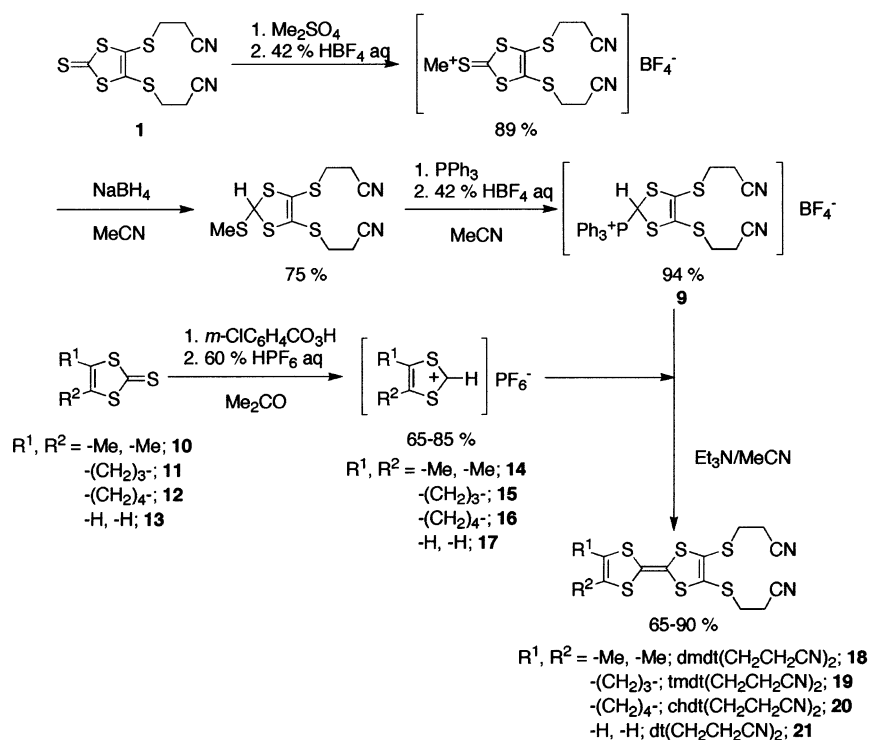
As shown in Scheme 1, cross-coupling reactions of a mixture of the 4,5-bis(2'-cyanoethylthio)-1,3-dithiol-

2-one (**2**) and 1,3-dithiole-2-thione (**3–5**) with *n*-propylthio, propylenedithio, and ethylenedioxy groups on the 4,5-positions were performed in neat trimethyl phosphite or triethyl phosphite at 110 °C. The asymmetrical TTFs (**6–8**) were obtained in good yields (55–65%) after a silica gel column-chromatographic separation (dichloromethane–*n*-hexane, chloroform, or dichloromethane as eluate), respectively, followed by the recrystallization from dichloromethane–ethanol, chloroform–ethanol, or dichloromethane–*n*-hexane solutions. It is important to note that, due to the high polarity of the cyanoethyl groups compared to the alkylthio or alkyloxy groups, good chromatographic separation of the reaction mixture could be achieved. Thus, this methodology has been successfully employed in the preparation of the bis-cyanoethyl protected TTFs with the alkylthio or alkyloxy substituents on the 4,5-positions.

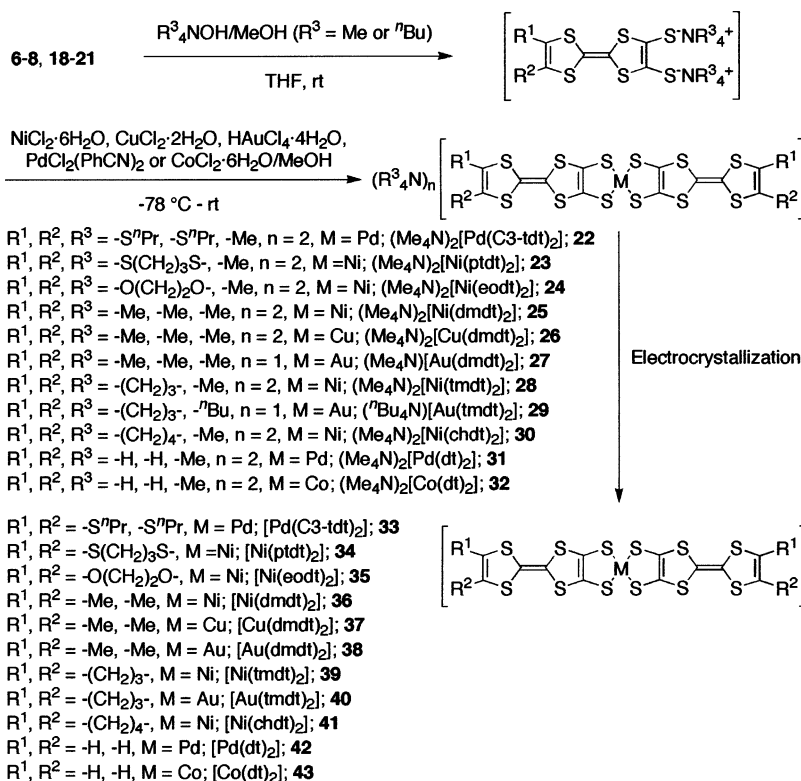
## 2.4.2. Pseudo-Wittig Reaction

It is generally difficult to obtain the asymmetrically bis-protected TTFs with the alkyl substituents in sufficient yields by the cross-coupling reaction using trialkyl phosphite. To prepare such compounds in higher yield, we turned our attention to the pseudo-Wittig condensation between the triphenylphosphonium tetrafluoroborate salt<sup>37</sup> (**9**) and the 1,3-dithiolium hexafluorophosphate salt<sup>39</sup> (**14–17**) having the alkyl substituents on the 4,5-positions according to the synthetic procedure reported by Becher et al.<sup>37</sup> Compound **9** was obtained in a three-step synthesis from 4,5-bis(2'-cyanoethylthio)-1,3-dithiole-2-thione (**1**) in an overall yield of 63%, as shown in Scheme 2. On the other hand, the peracid oxidation of the 1,3-dithiole-2-thione derivatives (**10–13**) using *m*-chloroperbenzoic acid in acetone at 0 °C and the subsequent addition of an aqueous solution of 60%

Scheme 2



## Scheme 3



hexafluorophosphoric acid gave the 1,3-dithiolium hexafluorophosphate salt (**14–17**) in 65–85% yields (see also Scheme 2). Because the cyanoethyl protective group is inactive to triethylamine, the asymmetrically bis-protected TTFs can be prepared successfully by the pseudo-Wittig reaction. Thus, the bis-cyanoethylthio substituted TTFs (**18–21**) were isolated from the reaction of the triphenylphosphonium salt (**9**) and 1,3-dithiolium salts (**14–17**) with triethylamine in acetonitrile at room temperature in 65–90% yields by recrystallization from dichloromethane–*n*-hexane or methanol after the separation by column chromatography (silica gel, dichloromethane, or dichloromethane–*n*-hexane).

#### 2.4.3. Syntheses of Neutral Metal Complexes

In the bis-cyanoethylthio substituted TTFs (**6–8**, **18–21**), the cyanoethyl groups are used to protect a dithiolate ligand function and can be removed with an excess of basic reagents. Thus, the deprotection of the cyanoethyl group creates the coordination ability of the dithiolate ligands toward a central metal atom.<sup>25,40–42</sup> As shown in Scheme 3, all of the dianionic and monoanionic metal complexes (**22–32**) were synthesized by almost the same methods under a strictly inert atmosphere using the Schlenk technique because the anionic states of the metal complexes are quite sensitive to oxygen. The dianionic and monoanionic metal complexes coordinated by two TTFs (**22–32**) were obtained as microcrystals by the deprotection of the bis-cyanoethylthio substituted TTFs (**6–8**, **18–21**) using a methanol solution of tetramethylammonium hydroxide or tetra-*n*-butylammonium hydroxide in dry tetrahydrofuran, followed by the addition of a dry methanol solution containing metal sources such as Ni<sup>II</sup>Cl<sub>2</sub>·6H<sub>2</sub>O,

Cu<sup>II</sup>Cl<sub>2</sub>·2H<sub>2</sub>O, HAu<sup>III</sup>Cl<sub>4</sub>·4H<sub>2</sub>O, Pd<sup>II</sup>Cl<sub>2</sub>(PhCN)<sub>2</sub>, or Co<sup>II</sup>Cl<sub>2</sub>·6H<sub>2</sub>O at –78 °C and a gradual temperature increase to room temperature.

The neutral metal complexes consisting of a single-component molecule (**33–43**) were obtained electrochemically from a 20% diethyl ether–acetonitrile, acetonitrile, tetrahydrofuran, dichloromethane, or benzonitrile solution containing the dianionic or monoanionic species (**22–32**) and the supporting electrolytes such as barium trithiocarbonate, tetra-*n*-butylammonium perchlorate, or tetra-*n*-butylammonium hexafluorophosphate in a standard H-type cell using two platinum electrodes (1 mm i.d. wires) at room temperature or 40 °C within several weeks by applying a constant current of 0.1–0.5 μA or a regulated voltage of 1.0 V between the two electrodes with a constant voltage supply, respectively (see also Scheme 3). Table 2 shows the conditions of electrochemical syntheses of neutral metal complexes. Crystals good enough to perform the single-crystal X-ray structure analysis were obtained for the metal complexes **33**, **34**, **36**, **37**, and **39**, while the other metal complexes (**35**, **38**, and **40–43**) were obtained as microcrystals by electrochemical oxidation. The obtained metal complexes (**33–43**) were insoluble in conventional organic solvents and comparatively stable in air.

#### 2.5. The First Single-Component Molecular Metal, [Ni(tmdt)<sub>2</sub>]

Extended π systems, with many sulfur atoms in the dithiolate ligands, have been thought to be of interest from the standpoint that the electrons are delocalized in the axis directions of the ligands, resulting in not only the decreases of the HOMO–

**Table 2. Electrochemical Oxidation of Metal Complexes**

anionic complex	electrolyte	conditions	product	$\rho$ (300 K)
(Me <sub>4</sub> N) <sub>2</sub> [Ni(dmdt) <sub>2</sub> ]	( <sup>n</sup> Bu <sub>4</sub> N)PF <sub>6</sub> (50 mg)	MeCN (0.2 $\mu$ A, 14 days)	[Ni(dmdt) <sub>2</sub> ]	300-400 S cm <sup>-1</sup> metallic down to 230 K
(Me <sub>4</sub> N) <sub>2</sub> [Pd(dmdt) <sub>2</sub> ]	(Me <sub>4</sub> N)Cl (50 mg)	MeCN (0.4 $\mu$ A, 10 days)	[Pd(dmdt) <sub>2</sub> ]	150 S cm <sup>-1</sup> semiconductor
(Me <sub>4</sub> N) <sub>2</sub> [Ni(tmdt) <sub>2</sub> ]	( <sup>n</sup> Bu <sub>4</sub> N)ClO <sub>4</sub> (50 mg)	MeCN (0.2 $\mu$ A, 14 days)	[Ni(tmdt) <sub>2</sub> ]	400 S cm <sup>-1</sup> metallic down to 0.6 K
(Me <sub>4</sub> N) <sub>2</sub> [Co(dmdt) <sub>2</sub> ]	( <sup>n</sup> Bu <sub>4</sub> N) (70 mg)	MeCN (0.3-0.9 $\mu$ A, 14 days)	[Co(dmdt) <sub>2</sub> ]	0.05 S cm <sup>-1</sup> semiconductor, $E_a = 85$ meV
(Me <sub>4</sub> N) <sub>2</sub> [Co(tmdt) <sub>2</sub> ]	( <sup>n</sup> Bu <sub>4</sub> N)PF <sub>6</sub> (80 mg)	MeCN (0.3-0.9 $\mu$ A, 14 days)	[Co(tmdt) <sub>2</sub> ]	1.5 S cm <sup>-1</sup> semiconductor, $E_a = 24$ meV
(Me <sub>4</sub> N) <sub>2</sub> [Cu(dmdt) <sub>2</sub> ]	( <sup>n</sup> Bu <sub>4</sub> N)PF <sub>6</sub> (50 mg)	THF (0.4 $\mu$ A, 10 days)	[Cu(dmdt) <sub>2</sub> ]	3.0 S cm <sup>-1</sup> semiconductor, $E_a = 40$ meV
(Me <sub>4</sub> N) <sub>2</sub> [Cu(tmdt) <sub>2</sub> ]	(Me <sub>4</sub> N)Cl (50 mg)	MeCN (0.4 $\mu$ A, 10 days)	[Cu(tmdt) <sub>2</sub> ]	5.1 S cm <sup>-1</sup> semiconductor, $E_a = 63$ meV
( <sup>n</sup> Bu <sub>4</sub> N)[Au(tmdt) <sub>2</sub> ]	( <sup>n</sup> Bu <sub>4</sub> N)ClO <sub>4</sub> (80 mg)	THF (0.2 $\mu$ A, 21 days)	[Au(tmdt) <sub>2</sub> ]	15 S cm <sup>-1</sup> $E_a = 20$ meV (300–50 K)
(Me <sub>4</sub> N)[Au(dmdt) <sub>2</sub> ]	( <sup>n</sup> Bu <sub>4</sub> N)ClO <sub>4</sub> (80 mg)	CH <sub>2</sub> Cl <sub>2</sub> (0.2 $\mu$ A, 21 days)	[Au(dmdt) <sub>2</sub> ]	12 S cm <sup>-1</sup> $E_a = 9$ meV (300–50 K)
(Me <sub>4</sub> N) <sub>2</sub> [Ni(dt) <sub>2</sub> ]	( <sup>n</sup> Bu <sub>4</sub> N)ClO <sub>4</sub> (50 mg)	MeCN (0.5 $\mu$ A, 14 days)	[Ni(dt) <sub>2</sub> ]	16 S cm <sup>-1</sup> semiconductor, $E_a = 35$ meV
(Me <sub>4</sub> N) <sub>2</sub> [Pd(dt) <sub>2</sub> ]	( <sup>n</sup> Bu <sub>4</sub> N)ClO <sub>4</sub> (50 mg)	THF (0.2 $\mu$ A, 10 days)	[Pd(dt) <sub>2</sub> ]	0.3 S cm <sup>-1</sup> semiconductor, $E_a = 94$ meV
(Me <sub>4</sub> N) <sub>2</sub> [Co(dt) <sub>2</sub> ]	( <sup>n</sup> Bu <sub>4</sub> N)ClO <sub>4</sub> (80 mg)	PhCN (0.5 $\mu$ A, 14-21 days)	[Co(dt) <sub>2</sub> ]	19 S cm <sup>-1</sup> (metal)
(Me <sub>4</sub> N) <sub>2</sub> [Ni(eodt) <sub>2</sub> ]	( <sup>n</sup> Bu <sub>4</sub> N)ClO <sub>4</sub> (80 mg)	PhCN (0.5 mA, 21-28 days)	[Ni(eodt) <sub>2</sub> ]	8 S cm <sup>-1</sup> metallic down to 120 K
(Me <sub>4</sub> N) <sub>2</sub> [Ni(chdt) <sub>2</sub> ]	( <sup>n</sup> Bu <sub>4</sub> N)PF <sub>6</sub> (80 mg)	PhCN (1.0 V, 40 °C, 21–28 days)	[Ni(chdt) <sub>2</sub> ]	2 S cm <sup>-1</sup> semiconductor, $E_a = 38$ meV
(Me <sub>4</sub> N) <sub>2</sub> [Ni(hfdt) <sub>2</sub> ]	( <sup>n</sup> Bu <sub>4</sub> N)PF <sub>6</sub> (80 mg)	PhCl (1.0 $\mu$ A, 14 days)	[Ni(hfdt) <sub>2</sub> ]	$1.4 \times 10^{-4}$ S cm <sup>-1</sup> semiconductor, $E_a = 22$ meV
(Me <sub>4</sub> N)[Au(hfdt) <sub>2</sub> ]	( <sup>n</sup> Bu <sub>4</sub> N)PF <sub>6</sub> (80 mg)	PhCl (1.0 $\mu$ A, 14 days)	[Au(hfdt) <sub>2</sub> ]	$3.2 \times 10^{-3}$ S cm <sup>-1</sup> semiconductor, $E_a = 220$ meV
(Me <sub>4</sub> N)[Pd(C3-tdt) <sub>2</sub> ]	( <sup>n</sup> Bu <sub>4</sub> N)ClO <sub>4</sub> (60-80 mg)	MeCN (0.1 mA, 10 days)	[Pd(C3-tdt) <sub>2</sub> ]	$1.9 \times 10^{-2}$ S cm <sup>-1</sup> semiconductor $E_a = 34$ meV (300–120 K) $E_a = 11$ meV (120–80 K)
(Me <sub>4</sub> N)[Ni(ptdt) <sub>2</sub> ]	BaCS <sub>3</sub> (95 mg)	20% Et <sub>2</sub> O–MeCN (0.1 $\mu$ A, 63 days)	[Ni(ptdt) <sub>2</sub> ]	7 S cm <sup>-1</sup> semiconductor, $E_a = 30$ meV

LUMO gap and on-site Coulombic repulsions but also the increasing of 2D or 3D interactions due to the S...S contacts of the ligands. The trial to synthesize [Ni(S<sub>6</sub>C<sub>6</sub>(CF<sub>3</sub>)<sub>2</sub>)<sub>2</sub>] with di(trifluoromethyl)tetrathiafulvalenedithiolate ligands was performed by Engler et al. in 1979.<sup>43</sup> Neutral complexes [Ni(C<sub>6</sub>S<sub>8</sub>R)<sub>2</sub>] (R = Me, Et, <sup>n</sup>Bu) were electrical conductors.<sup>40,44</sup> The possibility of metallic conduction had been suggested in the crystal of the neutral [Ni(S<sub>8</sub>C<sub>6</sub>Me<sub>2</sub>)<sub>2</sub>] complex in the small temperature region 300–275 K [ $\sigma$ (RT) = 10<sup>-1</sup> S cm<sup>-1</sup>].<sup>40,44</sup> This value is 2 orders of magnitude larger than the room-temperature conductivity of neutral [Ni(dmit)<sub>2</sub>] ( $3.5 \times 10^{-3}$  S cm<sup>-1</sup>).<sup>45</sup> And the typical neutral metal bis-1,2-dithiolene complex shows a much smaller conductivity around 10<sup>-5</sup> or 10<sup>-6</sup> S cm<sup>-1</sup>.

The electrical conductivity of [Ni(ptdt)<sub>2</sub>] is 7 S cm<sup>-1</sup> at room temperature, which is extremely high for a neutral molecular crystal. The electrical resistivity shows a monotonic increase down to 60 K with a very small activation energy (0.03 eV) (Figure 4).<sup>28</sup> The molecular and crystal structures of neutral [Ni(ptdt)<sub>2</sub>] are indicated in Figure 5. Figure 6 shows the intermolecular overlaps in neutral [Ni(ptdt)<sub>2</sub>], which are larger than those in the monoanionic (Me<sub>4</sub>N)[Ni(ptdt)<sub>2</sub>] complex and also indicate that there are transverse interactions in both compounds.<sup>41</sup> This structural feature was very unusual, considering that the neutral molecule usually has no attractive interactions between the neighboring molecules except for

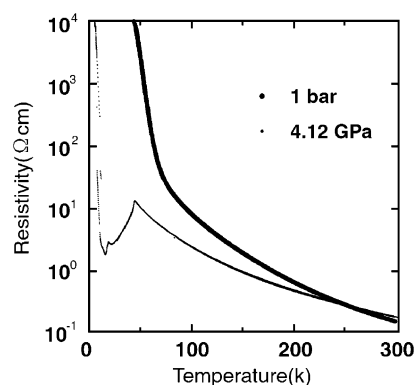


**Figure 4.** Resistivity of [Ni(ptdt)<sub>2</sub>] at ambient pressure and at high pressure (4.12 GPa). The phase transition from high-conducting state to low-conducting state was observed around 60 K at ambient pressure. The resistivity measurement at 4.12 GPa was performed with the four-probe method using the diamond-anvil cell.<sup>28</sup> During the cooling process, the resistivity was gradually increased down to 44 K, where the resistivity was 4  $\Omega$  cm. The resistivity then began to decrease, taking a minimum value of about 0.5  $\Omega$  cm. Below 16 K, the resistivity abruptly increased. There was a small apparent metallic region within the temperature range 44–20 K. High-pressure resistivity measurement was made up to 72 GPa; however, the resistivity could not be suppressed.

weak van der Waals interactions. From these results, we thought that the [Ni(ptdt)<sub>2</sub>] crystal would have a unique electronic structure which realized the close assembly of the molecules. The tight-binding band



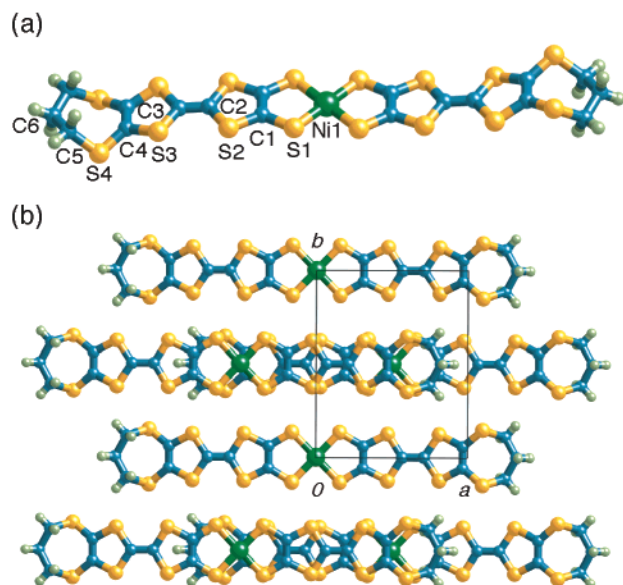


**Figure 5.** (a) Molecular structure and (b) crystal structure of  $[\text{Ni}(\text{ptdt})_2]$ . The  $[\text{Ni}(\text{ptdt})_2]$  molecule is almost planar except the terminal propylene group and forms a regular column along the  $a$  direction with an interplanar distance of 3.376 Å. The short S...S intermolecular distances indicate the existence of intermolecular interactions. Crystal data:  $\text{NiS}_{16}\text{C}_{18}\text{H}_{12}$ , monoclinic,  $C2/m$ ,  $a = 10.096(4)$  Å,  $b = 11.802(4)$  Å,  $c = 12.42(1)$  Å,  $\beta = 108.74(6)^\circ$ ,  $Z = 2$ ,  $V = 1401(1)$  Å<sup>3</sup>.

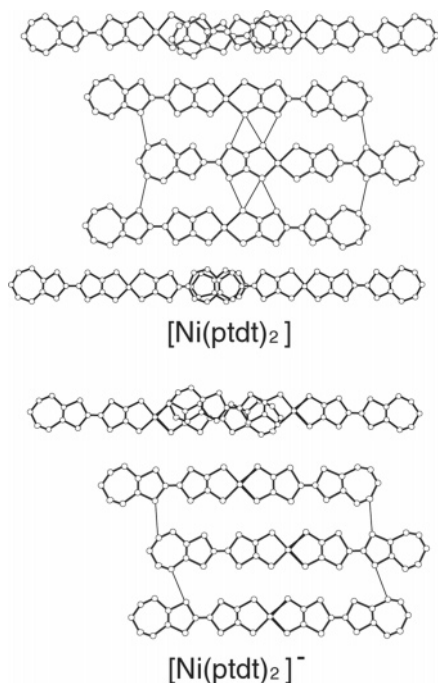


**Figure 6.** (top) Mode of overlaps, molecular arrangement along the transverse direction, and mode of overlaps along the long axis of the molecule in  $[\text{Ni}(\text{ptdt})_2]$ . (bottom) Mode of overlaps of  $[\text{Ni}(\text{ptdt})_2]^-$  anion and molecular arrangement along the transverse direction in  $(\text{Me}_4\text{N})[\text{Ni}(\text{ptdt})_2] \cdot \text{Me}_2\text{CO}$ .

structure calculation of  $[\text{Ni}(\text{ptdt})_2]$  indicated that the HOMO and the LUMO formed crossing bands, whose Fermi surfaces tended to vanish due to the HOMO–LUMO interactions. Only very small electron and hole pockets appeared in the Fermi surface due to the transverse interactions between neighboring columns (Figure 7). On the basis of these analyses,

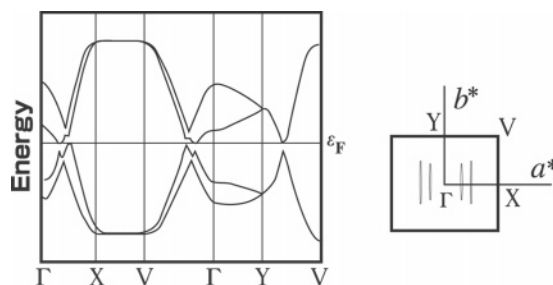


**Figure 7.** Band structure calculation indicating the crossing band formation of the HOMO and LUMO in  $[\text{Ni}(\text{ptdt})_2]$ . Band energies and Fermi surfaces were calculated by assuming the HOMO–LUMO gap = 0.12 eV. Only very small electron and hole pockets appeared in the Fermi surface due to the transverse interactions between neighboring columns.

the guiding principle for the development of molecular metals composed of single molecules was obtained.<sup>28</sup>

Then, we prepared a Ni complex with extended-TTF ligands, *tmdt*. Considering that the amplitudes of the HOMO and LUMO of  $[\text{Ni}(\text{ptdt})_2]$  are small for the sulfur atoms of the terminal propylenedithio group (see Figure 3c), the sulfur atoms in the terminal rings are not important in the construction of the metal band. Therefore, we selected a more planar and shorter extended-TTF ligand with a trimethylene group (or a dimethyl group) instead of alkylthio groups in order to increase molecular interactions. The crystal and the band structure analyses and the resistivity measurements of the crystal of  $[\text{Ni}(\text{tmdt})_2]$  revealed that we obtained the first 3D metal composed of single-component planar molecules.<sup>24,25</sup>

Crystal structure determination was performed using a black crystal with a size of  $0.1 \times 0.05 \times 0.03$  mm<sup>3</sup>. As the size of the crystal was very small, a diffraction experiment was made on a Rigaku MERCURY CCD system at 123 K to collect a sufficient number of reflections. The lattice constants are  $a = 6.376(3)$  Å,  $b = 7.359(1)$  Å,  $c = 12.012(7)$  Å,  $\alpha = 90.384(7)^\circ$ ,  $\beta = 96.688(4)^\circ$ ,  $\gamma = 103.587(4)^\circ$ , and  $V = 543.7(4)$  Å<sup>3</sup> with space group  $P\bar{1}$  and  $Z = 1$ . Neutral  $[\text{Ni}(\text{tmdt})_2]$  molecules crystallize into a very simple triclinic structure (Figure 8).<sup>24,25</sup> The unit cell contains only one molecule. The central Ni atoms are on the lattice points, and half of the molecule is crystallographically independent. The molecule is ideally planar even in the terminal trimethylene group, and the planar molecules are closely packed in the crystal plane (02 $\bar{1}$ ) (Figure 8b). The average Ni–S distance is 2.177(7) Å, and the S–Ni–S angle is 92.29(4) $^\circ$  at 123 K. The C=C bond length in the TTF skeleton is 1.362(5) Å. The bond lengths of neutral and dianionic  $[\text{Ni}(\text{tmdt})_2]$  and  $(\text{tBu}_4\text{N})_2[\text{Ni}(\text{tmdt})_2]$  are already compared in Table 1 (see section 2.3).  $[\text{Ni}(\text{tmdt})_2]$  molecules have S...S transverse short contacts (3.350(2)–3.675(2) Å) along the [100] direction, which is shown in Figure 9a. There are two types of overlap modes, and in both cases almost half of the molecules are overlapped. The average interplanar distance between the molecules on (0,0,0) and (1,1,1) is 3.677 Å, and that between molecules on (0,0,0) and (1,0,1) is

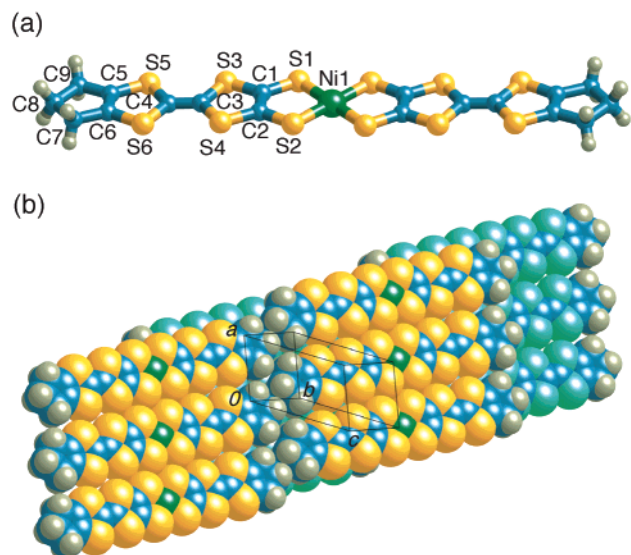


**Figure 8.** (a) Molecular structure and (b) crystal structure of  $[\text{Ni}(\text{tmdt})_2]$ . The molecule is ideally planar even in the terminal trimethylene group. Neutral molecules crystallize into a very simple triclinic structure, and the unit cell contains only one molecule. Molecules are closely packed to form the crystal plane (021).

3.346 Å, which are shown in Figure 9b. Figure 9c shows the end-on projection of  $[\text{Ni}(\text{tmdt})_2]$ . These structural features suggest that the system has 3D intermolecular interactions.

The single-crystal conductivity measurements of  $[\text{Ni}(\text{tmdt})_2]$  were made nearly along the  $a$ -axis down to 0.6 K using the four-probe method. The room-temperature conductivity was  $400 \text{ S cm}^{-1}$ , which is almost 1 order of magnitude greater than those of typical BEDT-TTF organic superconductors. The metallic behavior was observed down to 0.6 K (Figure 10a).<sup>24,25</sup> A compacted powder sample also gave high conductivity [ $\sigma(\text{RT}) = 200 \text{ S cm}^{-1}$ ] and exhibited metallic behavior down to 70 K, suggesting small anisotropy of the resistivity, which is consistent with the existence of 3D conduction paths (Figure 10a). Molecular crystals of single-component molecules have been considered to be typical crystals with inherent insulating properties. However,  $[\text{Ni}(\text{tmdt})_2]$  crystals have removed the boundary between molecular crystals and metallic crystals.

The susceptibility measured on a polycrystalline sample with a SQUID magnetometer within the temperature range 2–300 K exhibited a weakly temperature-dependent paramagnetic susceptibility ( $(2.6\text{--}3.1) \times 10^{-4} \text{ emu mol}^{-1}$ ), which is consistent with the metallic nature of the system (Figure 10b).

As shown in Figure 3c, the HOMO and LUMO of  $[\text{Ni}(\text{tmdt})_2]$  are similar to those of  $[\text{Ni}(\text{ptdt})_2]$ . However, the anisotropy of the intermolecular interactions, is of course, quite different from that of  $[\text{Ni}(\text{ptdt})_2]$ . The interstack overlap integrals are shown in Table 3. There are large overlap integrals along the [111] direction (B<sub>1</sub>, see Figure 9c) for the LUMO–LUMO ( $3.2 \times 10^{-3}$ ), for the HOMO–HOMO ( $-4.8 \times 10^{-3}$ ), for the HOMO–LUMO ( $4.1 \times 10^{-3}$ ), and for the LUMO–HOMO ( $-4.1 \times 10^{-3}$ ) interactions and along the [100] direction (A, see Figure 9c) for the LUMO–LUMO ( $1.8 \times 10^{-3}$ ) and for the

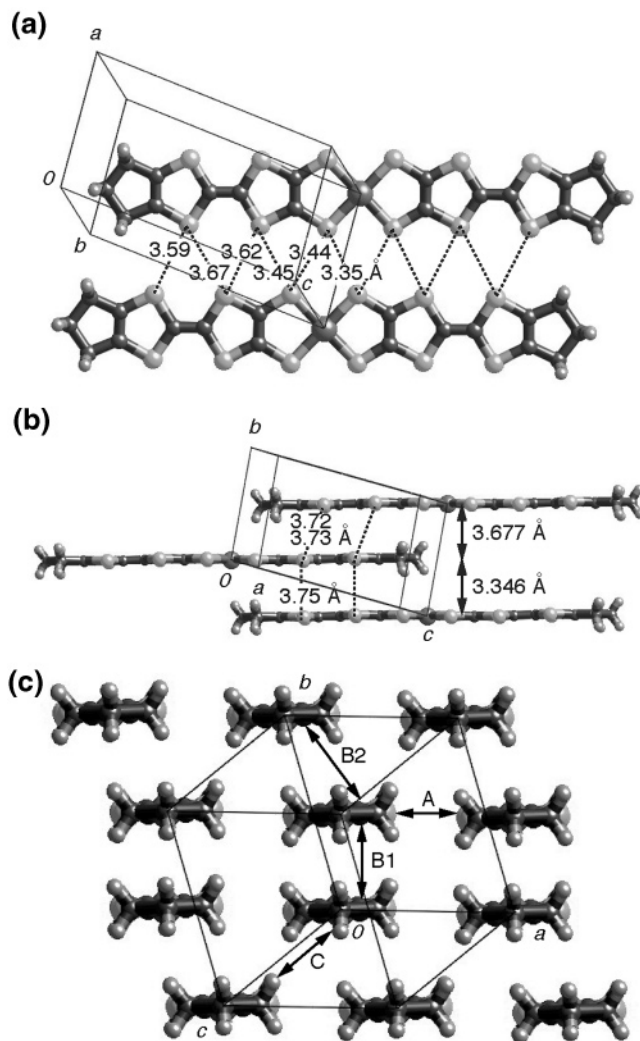


**Figure 9.** (a) Crystal structure of  $[\text{Ni}(\text{tmdt})_2]$  viewed along the perpendicular axis of the molecular plane and intermolecular S...S short contacts along the  $a$ -axis (3.35–3.67 Å). (b) Side view of the molecular stacking and interplanar distances with S...S short contacts. There are two types of overlap modes, and in both cases almost half of the molecules are overlapped. (c) End-on projection of  $[\text{Ni}(\text{tmdt})_2]$ . Overlap integrals in Table 3 were calculated along the directions A, B<sub>1</sub>, B<sub>2</sub>, and C.

HOMO–HOMO ( $2.8 \times 10^{-3}$ ) interactions, respectively. Large overlap integrals are also seen along the [001] direction (C, see Figure 9c) for the LUMO–LUMO ( $1.8 \times 10^{-3}$ ), for the HOMO–HOMO ( $-3.3 \times 10^{-3}$ ), for the HOMO–LUMO ( $2.4 \times 10^{-3}$ ), and for the LUMO–HOMO ( $-2.4 \times 10^{-3}$ ) interactions, respectively. These overlap integrals and the band structure of  $[\text{Ni}(\text{tmdt})_2]$  were calculated on the basis of the extended-Hückel parameters.<sup>46</sup> These results show that the system has 3D  $\pi$  bands. According to the previous discussion, a 3D system having large “transverse intermolecular interactions” in two directions is considered to be able to have fairly large Fermi surfaces even when the HOMO and LUMO form “crossing bands”. Extended Hückel MO calculations gave  $\Delta E$  of about 0.10 eV. But the band calculations were performed with varying  $\Delta E$  values because the precise estimation of the value of  $\Delta E$  is difficult. Fermi surfaces was obtained for  $\Delta E < 0.34 \text{ eV}$ . The calculated Fermi surfaces for  $\Delta E = 0.105 \text{ eV}$

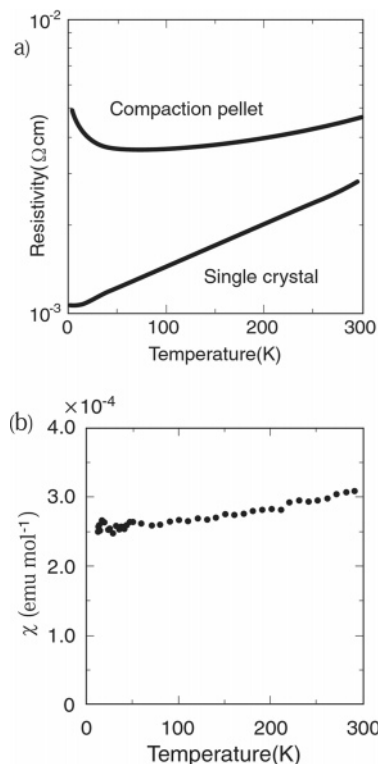


**Figure 10.** (a) Temperature dependence of resistivities of single crystals (approximately along the  $a$ -axis) of  $[\text{Ni}(\text{tmdt})_2]$ . The room-temperature conductivity was  $400 \text{ S cm}^{-1}$ , and  $[\text{Ni}(\text{tmdt})_2]$  retained metallic conductivity down to  $0.6 \text{ K}$ . A compaction pellet sample also gave high conductivity [ $\sigma(\text{RT}) = 200 \text{ S cm}^{-1}$ ] and exhibited metallic behavior down to  $70 \text{ K}$ , suggesting small anisotropy of the resistivity. (b) Magnetic susceptibility  $\chi$  of  $[\text{Ni}(\text{tmdt})_2]$  crystals. The susceptibility measured on a polycrystalline sample with a SQUID magnetometer within the temperature range  $2\text{--}300 \text{ K}$  exhibited a weakly temperature-dependent paramagnetic susceptibility ( $(2.6\text{--}3.1) \times 10^{-4} \text{ emu mol}^{-1}$ ), which is consistent with the metallic nature of the system.

**Table 3. Overlap Integrals of the HOMO and LUMO ( $\times 10^{-3}$ ) of  $[\text{Ni}(\text{tmdt})_2]$  at  $123 \text{ K}$**

	A	B1	B2	C
HOMO–HOMO	2.8	−4.8	0	−3.3
LUMO–LUMO	1.8	3.2	−0.3	1.8
HOMO–LUMO	0.07	4.1	−0.4	2.4
LUMO–HOMO	−0.07	−4.1	0.3	−2.4

are shown in Figure 11. Upper and lower bands are mixed around the Fermi energy ( $\epsilon_F$ ), owing to the mixing of HOMO and LUMO bands. The density of state (DOS) and the band energy dispersion curves are given in Figures 12 and 13, which show the crossing band character of the electronic structure.

Recently, direct experimental evidence for the Fermi surfaces in  $[\text{Ni}(\text{tmdt})_2]$  was obtained by detecting the quantum oscillations in magnetization, the dHvA effect. Torque magnetometry measurements of single crystals of  $[\text{Ni}(\text{tmdt})_2]$  using a sensitive microcantilever at low temperature in a high magnetic field revealed the presence of electron and hole Fermi surfaces. To compare the experimental results with electronic structure calculations, the local density approximation (LDA) calculations based on the *ab initio* plane-wave norm-conserved pseudopotential

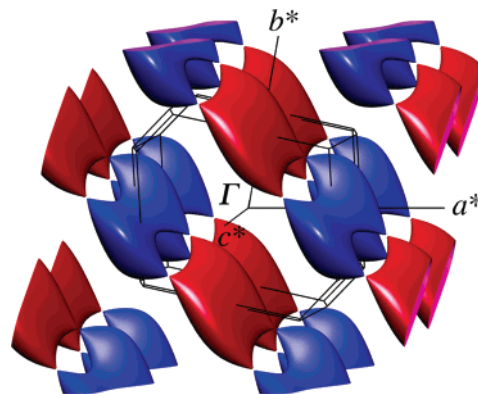


**Figure 11.** Calculated electron (red) and hole (blue) Fermi surfaces of  $[\text{Ni}(\text{tmdt})_2]$ . Calculations were made varying  $\Delta E$  by employing the parameters shown in ref 46. The HOMO–LUMO gap  $\Delta E$  is assumed as  $0.105 \text{ eV}$ . These Fermi surfaces well conform with those obtained on the basis of dHvA oscillation.

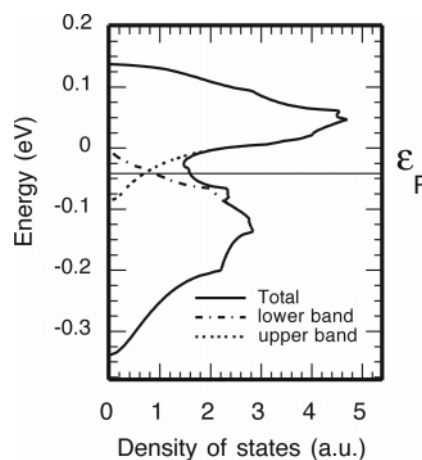


**Figure 12.** Density of states of  $[\text{Ni}(\text{tmdt})_2]$  calculated assuming  $\Delta E$  of  $0.105 \text{ eV}$ . Lower band and upper band contributions are shown by dotted lines. Bandwidth is  $0.48 \text{ eV}$ .

method with Troullier–Martins potentials were performed by Ishibashi et al.<sup>26</sup> The HOMO and LUMO bandwidths were estimated to be  $0.707$  and  $0.577 \text{ eV}$ , respectively, and the two bandwidths had an overlap of  $0.195 \text{ eV}$ , which is consistent with the previous calculations of Rovira et al.<sup>47</sup> The revised extended-Hückel tight-binding band calculations gave essentially the same topology for the Fermi surfaces.<sup>26</sup> An example of the extremal orbit is illustrated in Figure 14 with the calculated Fermi surfaces. The blue and red closed surfaces represent the hole and electron Fermi pockets, and the volume of each pocket occupies  $3.5\%$  of the first Brillouin zone. The presence of the electron and hole Fermi surfaces revealed by the dHvA oscillatory signals corresponds well with the Fermi surfaces obtained by these band structure calculations, which indicate that both electron and hole 3D Fermi surfaces unambiguously exist in this  $[\text{Ni}(\text{tmdt})_2]$ .

## 2.6. Analogous Single-Component Molecular Metals

Metallic behavior was also found in the crystal of an analogous molecule,  $[\text{Ni}(\text{dmdt})_2]$  (dmdt = dimethyltetrathiafulvalenedithiolate). The room-tempera-

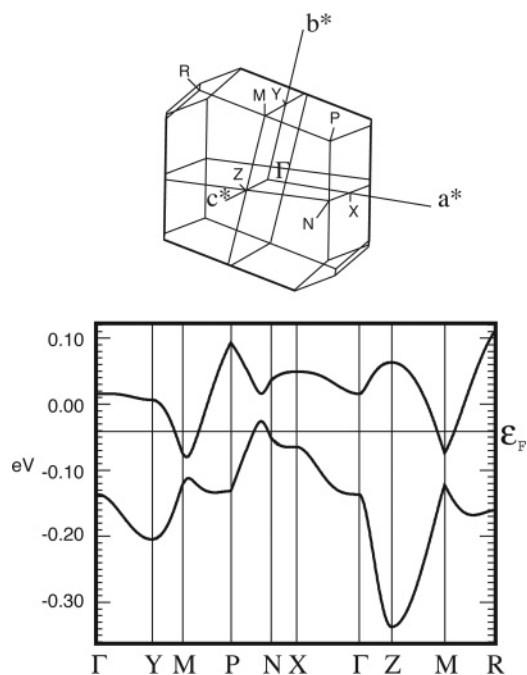


**Figure 13.** Band energy dispersion curves of  $[\text{Ni}(\text{tmdt})_2]$ . The crossing band character of the electronic structure of  $[\text{Ni}(\text{tmdt})_2]$  is clearly shown. Upper and lower bands are mixed around the Fermi energy ( $\epsilon_F$ ) and form electron and hole Fermi surfaces.

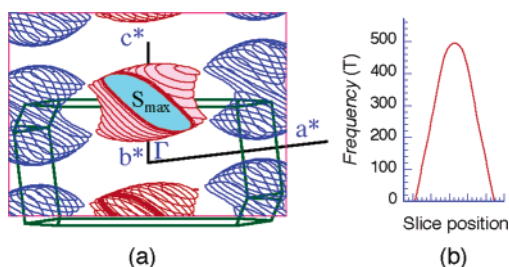


**Figure 14.** (a) Hole (blue) and electron (red) Fermi surfaces and the first Brillouin zone of  $[\text{Ni}(\text{tmdt})_2]$ . (b) Extremal electron orbits for the field applied parallel to  $b^*$ . The corresponding extremal cross section size was calculated by slicing Fermi surfaces.

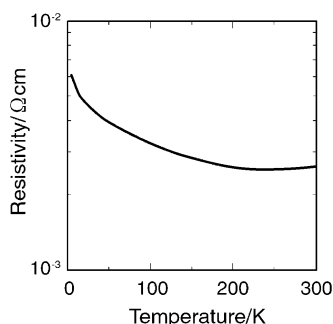


**Figure 15.** Temperature dependence of the resistivities of compacted pellet samples of  $[\text{Ni}(\text{dmdt})_2]$  showing metallic behavior down to 230 K. The room-temperature conductivity was  $(3\text{--}4) \times 10^2 \text{ S cm}^{-1}$ . Below 230 K the resistivity gradually increased but was still highly conducting even at 4 K.

ture conductivity measured on the compressed pellet sample was  $(3\text{--}4) \times 10^2 \text{ S cm}^{-1}$  and retained metallic behavior down to 230 K. Below this temperature, the resistivity gradually increased but was still highly conductive even at 4 K (Figure 15). The magnetic

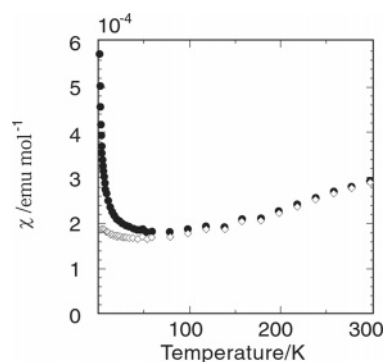


**Figure 16.** Magnetic susceptibility measured on a polycrystalline sample from room temperature to 2 K. The magnetic susceptibility was  $2.9 \times 10^{-4} \text{ emu mol}^{-1}$  at room temperature and gradually decreased with lowering temperature. The magnetic properties are quite similar to those of  $[\text{Ni}(\text{tmdt})_2]$ .

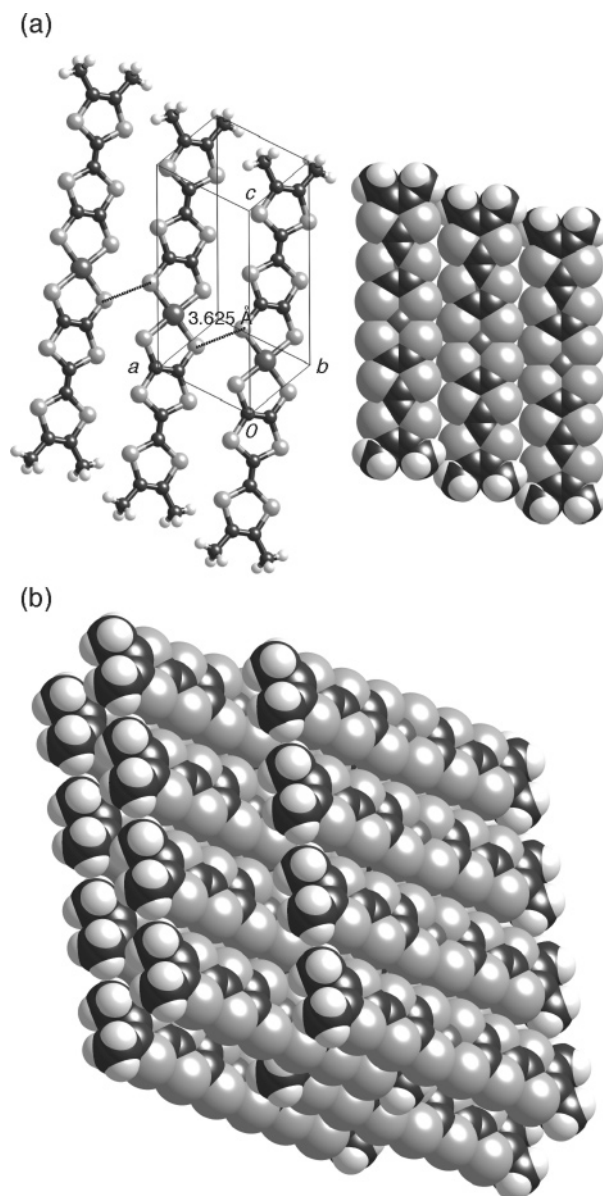


**Figure 17.** (a) Crystal structure and molecular arrangement viewed along the perpendicular axis of the molecule. (b) View of the molecular stacking of  $[\text{Ni}(\text{dmdt})_2]$ . The unit cell contains only one molecule. The central Ni atoms are on the lattice points. The planar molecules are closely packed in the crystal.

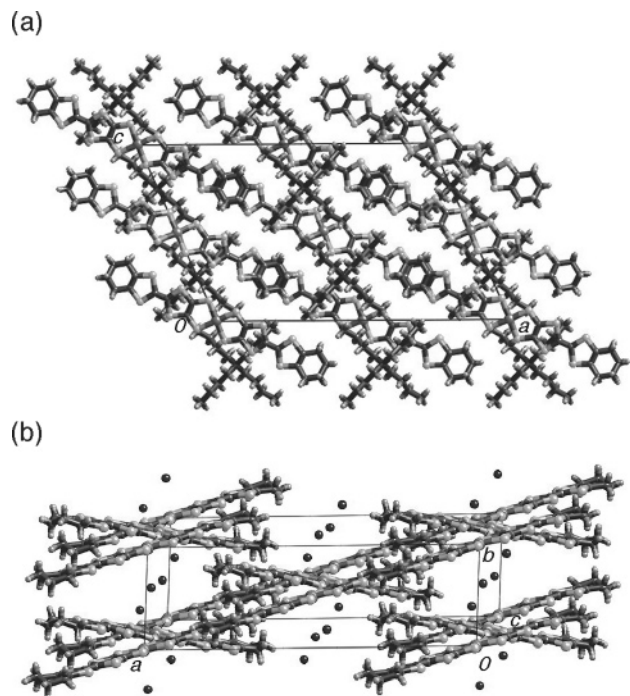


**Figure 18.** (a) Crystal structure of  $(n\text{Bu}_4\text{N})_2[\text{Ni}(\text{chdt})_2]$  projected onto the  $ac$ -plane. (b) One-dimensional array with a constant interval of  $(n\text{Bu}_4\text{N})_2[\text{Ni}(\text{chdt})_2]$  viewed along the  $c$ -axis. Each  $[\text{Ni}(\text{chdt})_2]^-$  anion is arranged along the diagonal direction in the  $ab$ - and  $ac$ -planes with an overlap of only the terminal cyclohexene rings to each other. Crystal data:  $\text{C}_{36}\text{H}_{52}\text{S}_{12}\text{NiN}$ , monoclinic,  $C2/c$ ,  $a = 29.018(4)$  Å,  $b = 8.5822(8)$  Å,  $c = 19.133(2)$  Å,  $\beta = 113.628(5)^\circ$ ,  $Z = 4$ ,  $V = 4365.5(9)$  Å<sup>3</sup>.

susceptibility was measured on a polycrystalline sample from room temperature to 2 K. The magnetic properties are quite similar to those of  $[\text{Ni}(\text{tmdt})_2]$ . The magnetic susceptibility was  $2.9 \times 10^{-4}$  emu mol<sup>-1</sup> at room temperature and gradually decreased with lowering temperature (Figure 16). The single-crystal structure determination of  $[\text{Ni}(\text{dmdt})_2]$  was performed on the Rigaku CCD X-ray system, and the crystal structure is shown in Figure 17a. Crystal data:  $\text{C}_{16}\text{H}_{12}\text{S}_{12}\text{Ni}$ , triclinic,  $P\bar{1}$ ,  $a = 6.620(4)$  Å,  $b = 7.615(6)$  Å,  $c = 11.561(8)$  Å,  $\alpha = 86.46(7)^\circ$ ,  $\beta = 79.43(6)^\circ$ ,  $\gamma = 74.22(5)^\circ$ ,  $Z = 1$ ,  $V = 551.2(8)$  Å<sup>3</sup>. Similar to  $[\text{Ni}(\text{tmdt})_2]$ , neutral  $[\text{Ni}(\text{dmdt})_2]$  molecules crystallize into a very simple triclinic structure (Figure 17a).<sup>48</sup> The unit cell contains only one molecule. The central Ni atoms are on the lattice points, and half of the molecule is crystallographically independent. The planar molecules are closely packed in the crystal (Figure 17b). The average Ni–S distance is 2.173 Å, and the S–Ni–S angle is  $92.2(2)^\circ$ . These results show that the crystal of  $[\text{Ni}(\text{dmdt})_2]$  is the second single-component molecular metal.

New nickel bis(dithiolene) complexes with the ligands containing six-membered rings such as a cyclohexeno-fused or ethylenedioxy-substituted TTF skeleton,  $(n\text{Bu}_4\text{N})[\text{Ni}(\text{chdt})_2]$ ,  $[\text{Ni}(\text{chdt})_2]$ ,  $(n\text{Bu}_4\text{N})[\text{Ni}(\text{eodt})_2]$ , and  $[\text{Ni}(\text{eodt})_2]$ , were synthesized, and their crystal structures and physical properties were examined (chdt = cyclohexenotetrathiafulvalenedithiolate, eodt = ethylenedioxytetrathiafulvalenedithiolate).<sup>49</sup> The crystal structures of the monoanionic complexes  $(n\text{Bu}_4\text{N})[\text{Ni}(\text{chdt})_2]$  and  $(n\text{Bu}_4\text{N})[\text{Ni}(\text{eodt})_2]$

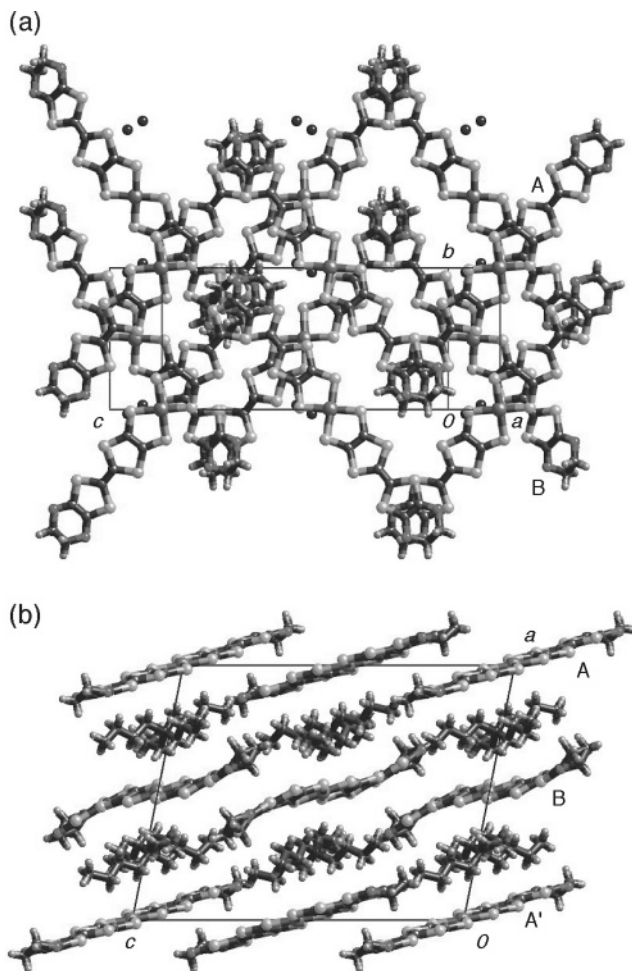


**Figure 19.** (a) Anion arrangement projected onto the  $bc$ -plane in  $(n\text{Bu}_4\text{N})[\text{Ni}(\text{eodt})_2]$ . (b) Crystal structure of  $(n\text{Bu}_4\text{N})[\text{Ni}(\text{eodt})_2]$  projected onto the  $ac$ -plane. Crystal data:  $\text{C}_{32}\text{H}_{44}\text{S}_{12}\text{NiN}$ , monoclinic,  $P2/c$ ,  $a = 18.406(1)$  Å,  $b = 9.8418(5)$  Å,  $c = 23.444(2)$  Å,  $\beta = 101.280(4)^\circ$ ,  $Z = 4$ ,  $V = 4164.8(5)$  Å<sup>3</sup>.

were determined (Figures 18 and 19). Both monoanionic species have sandwiched structures, in which the chains or layers of the nickel complexes and cations are arranged alternately. Thus, the monoanionic species indicated that there is no interchain or interlayer S $\cdots$ S contact less than the sum of van der Waals radii (3.7 Å) between the complex molecules along the sandwiched directions. On the other hand, the close S $\cdots$ S distances were observed only in the transverse direction. The magnetic properties of the monoanionic species  $(n\text{Bu}_4\text{N})[\text{Ni}(\text{chdt})_2]$  and  $(n\text{Bu}_4\text{N})[\text{Ni}(\text{eodt})_2]$  indicated the paramagnetism with the antiferromagnetic interaction between the anions of  $S = 1/2$  states. The magnetic behavior of the monoanionic species  $(n\text{Bu}_4\text{N})[\text{Ni}(\text{chdt})_2]$  is in good agreement with the Bonner–Fisher model ( $J/k_B = -28$  K), while  $(n\text{Bu}_4\text{N})[\text{Ni}(\text{eodt})_2]$  exhibits the Curie–Weiss behavior ( $C = 0.376$  K emu mol<sup>-1</sup> and  $\theta = -4.6$  K). The neutral species  $[\text{Ni}(\text{chdt})_2]$  and  $[\text{Ni}(\text{eodt})_2]$  showed fairly large room-temperature electrical conductivities (1–10 S cm<sup>-1</sup>), although the measurements were made on the compressed pellets of samples. Especially, the complex  $[\text{Ni}(\text{eodt})_2]$  showed metallic temperature dependence down to 120 K and retained high conductivity even at 0.6 K [ $\sigma(0.6\text{ K})/\sigma(\text{RT}) \approx 1/30$ ] (Figure 20), which

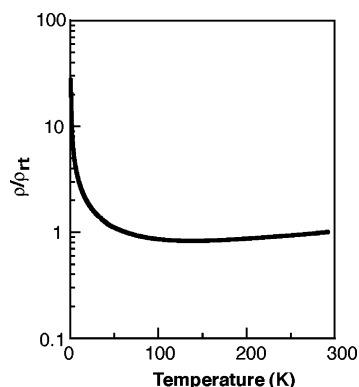


**Figure 20.** Temperature dependence of electrical resistivities of the neutral nickel complex  $[\text{Ni}(\text{eodt})_2]$ . Despite the compressed pellet sample, the neutral  $[\text{Ni}(\text{eodt})_2]$  showed fairly large room-temperature electrical conductivities ( $1\text{--}10\text{ S cm}^{-1}$ ) and the resistivity of the neutral complex decreased down to  $\sim 120\text{ K}$ . Below  $120\text{ K}$  the resistivity increased very slowly and the sample retained fairly high conductivity even at  $0.6\text{ K}$  [ $\sigma(0.6\text{ K})/\sigma(\text{RT}) \approx 1/30$ ]. These data show the system to be essentially metallic down to very low temperature.

suggested the system to be essentially metallic down to very low temperature.

### 3. Development of New Functional Single-Component Molecular Conductors with Extended-TTF Dithiolate Ligands

Since single-component molecular metals have been developed, it is worthwhile to consider new possibilities for the development of new functional molecules provided by these discoveries. (1) Although the resistivity measurements were made down to about  $0.5\text{ K}$ , superconductivity has not been discovered yet. As mentioned above, the Fermi surfaces of a  $[\text{Ni}(\text{tmdt})_2]$  crystal tend to be diminished by the HOMO–LUMO interaction due to the crossing band properties of the electronic structure. If we can obtain a single-component molecular metal with a large Fermi surface (or a large DOS at Fermi energy  $D(\epsilon_F)$ ) by controlling the sign and the magnitude of intermolecular HOMO–HOMO, LUMO–LUMO, and HOMO–LUMO interactions, it might be possible to prepare a single-component molecular superconductor. (2) Similar to metal elements such as Na and Cu,  $[\text{Ni}(\text{tmdt})_2]$  molecules self-assemble to form metallic crystals. However, needless to say, there are many differences between an atom and a molecule. Although a nonmagnetic element such as Na and Cu cannot be changed into a magnetic element such as Fe and Co,  $[\text{Ni}(\text{tmdt})_2]$  can be converted into a magnetic molecule by replacing the central  $\text{Ni}^{2+}$  atom with magnetic atoms such as  $\text{Cu}^{2+}$  and  $\text{Co}^{2+}$ . It is well-known that the Curie temperature ( $T_c$ ) for ferromagnetic crystals composed of single organic molecules such as *p*-nitrophenyl nitronyl nitroxide is very low,<sup>50</sup> but the transition temperature of a molecular ferromagnet is expected to be much higher if the intermolecular magnetic interaction is mediated by conduction electrons. Therefore, magnetic molecular conductors with high  $T_c$  values will be expected when using magnetic analogues of  $[\text{Ni}(\text{tmdt})_2]$ .

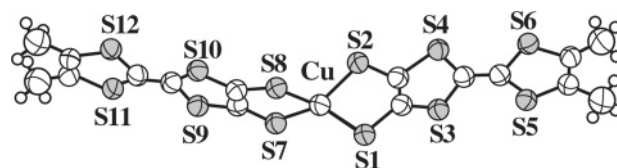


**Figure 21.** Molecular structure of a dianionic copper complex in  $(n\text{Bu}_4\text{N})_2[\text{Cu}(\text{dmdt})_2]$ . The coordination geometry of copper is greatly distorted from planar, and the molecular long axis is curved. The dihedral angle between the least-squares planes of two extended-TTF ligands is  $33.5^\circ$ .

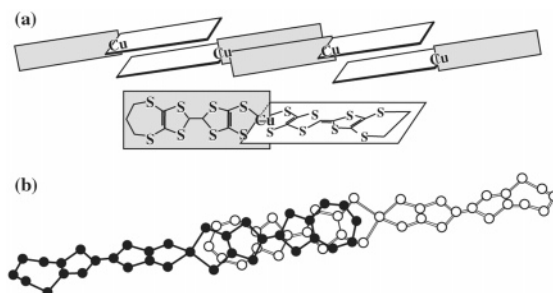


**Figure 22.** (a) Schematic drawing of the molecular arrangement and (b) overlapping mode of  $(\text{Ph}_4\text{P})_2[\text{Cu}(\text{ptdt})_2] \cdot 1.2(\text{Me}_2\text{CO})$ . The  $\pi$ -conjugated systems of the ptdt ligand are large enough to form conduction pathways in the crystal.

In this section, we will mention our recent topics in the development of single-component molecular conductors based on bis(tetrathiafulvalenedithiolato)-metal (Cu, Co, Au, Pd) complexes.

#### 3.1. Single-Component Paramagnetic Conductor $[\text{Cu}(\text{dmdt})_2]$

The structural, electrical, and magnetic properties of crystals composed of a single-component copper complex with an extended-TTF ligand,  $[\text{Cu}(\text{dmdt})_2]$ , were examined to contribute to clarifying the possibility of single-component magnetic molecular conductors.<sup>31</sup> Figure 21 shows the molecular structure of the dianionic complex,  $[\text{Cu}(\text{dmdt})_2]^{2-}$ , in  $(n\text{Bu}_4\text{N})_2[\text{Cu}(\text{dmdt})_2]$ .<sup>31</sup> The coordination geometry of copper is a distorted tetrahedral symmetry, and the molecular long axis is curved. The dihedral angle between the least squares planes of two extended-TTF ligands is  $33.5^\circ$ , which is smaller than those of the other copper complexes such as  $[\text{Cu}(\text{ptdt})_2]^{2-}$  ( $54.2^\circ$ ) (Figure 22) and  $[\text{Cu}(\text{dmit})_2]^{2-}$  ( $57.3^\circ$ ).<sup>41,51</sup> In the crystal structure determination of  $(\text{Ph}_4\text{P})_2[\text{Cu}(\text{ptdt})_2] \cdot 1.2(\text{Me}_2\text{CO})$ , we found that the geometry around the Cu atom is tetrahedral but the ptdt ligands are large enough to form conduction pathways, which showed the possibility of novel 2D or 3D intermolecular contacts through ptdt ligands.<sup>41</sup> The schematic stacking pattern is shown in Figure 22a. In the case of  $[\text{epy}]_2[\text{Cu}(\text{dmit})_2]$  (epy = ethyl-pyridinium), owing to the small size of the ligand, the stacking of  $[\text{Cu}(\text{dmit})_2]$  is only via one side of the ligand, which prevents the formation of a good conduction pathway.<sup>51</sup>

On the other hand, as shown in Figure 23a, the molecular structure of the neutral complex  $[\text{Cu}(\text{dmdt})_2]$  is also nonplanar, while the dmdt ligand moiety is almost ideally planar and has a straight molecular long axis. The dihedral angle between the

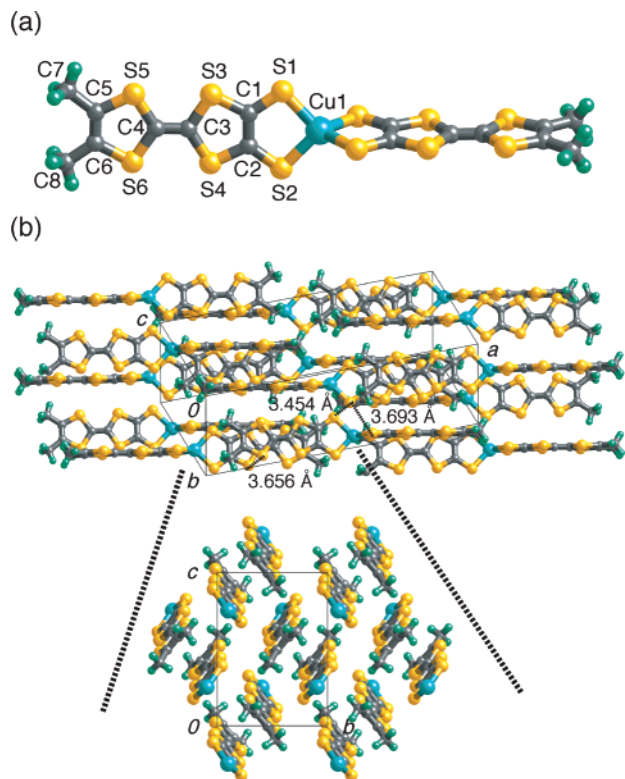


**Figure 23.** (a) Molecular structure and (b) crystal structure of  $[\text{Cu}(\text{dmdt})_2]$ . The  $\text{S}\cdots\text{S}$  contacts are shown as dotted lines. The lowest part of the figure presents the arrangement of the molecules projected along the molecular long axis. The neutral molecules take an unprecedented molecular arrangement. One of the ligands of  $[\text{Cu}(\text{dmdt})_2]$  overlaps, face-to-face, with the ligand of the adjacent molecule, and the opposite-side ligand overlaps with the ligand of the third molecule.

ligand planes is  $80.29^\circ$ . In the case of the neutral  $[\text{Cu}(\text{dmdt})_2]$ , both ligands overlap with adjacent ligands and form a good conduction pathway. As shown in Figure 23b, the neutral molecules take an unprecedented molecular arrangement. The molecular arrangement in  $[\text{Cu}(\text{dmdt})_2]$  is completely different from that in  $[\text{Ni}(\text{tmdt})_2]$ , where, ideally, planar molecules are closely packed to form a 3D metallic band.<sup>24,25</sup> One of the ligands of  $[\text{Cu}(\text{dmdt})_2]$  overlaps face-to-face with the ligand of the adjacent molecule, and the opposite side ligand overlaps with the ligand of the third molecule. Thus, the dmdt ligands take an arrangement similar to that of “ $\kappa$ -type organic superconductors”, which was first found in 1987.<sup>10</sup>  $\text{S}\cdots\text{S}$  contacts shorter than 3.45 Å exist between adjacent molecules, as shown in Figure 23b. The short  $\text{S}\cdots\text{S}$  contacts exist not only in the layer with a  $\kappa$ -type ligand arrangement but also between the adjacent layers. These structural features suggest the possibility of the existence of 3D conduction pathways.

The resistivity measurements on the crystals of  $[\text{Cu}(\text{dmdt})_2]$  showed fairly high conductivity, though the quality of the crystals was poor (about  $3 \text{ S cm}^{-1}$  at room temperature). Despite the apparent semi-conducting properties, the activation energy was very small (40 meV), while the crystal of  $(^n\text{Bu}_4\text{N})_2[\text{Cu}(\text{dmdt})_2]$  was found to be an insulator. The magnetic susceptibilities of crystals  $[\text{Cu}(\text{dmdt})_2]$  and  $(^n\text{Bu}_4\text{N})_2$ -

**Table 4.** Average Bond Lengths (Å) of the Dianion ( $n = 2^-$ ) and Neutral ( $n = 0$ )  $[\text{Cu}(\text{dmdt})_2]^n$

$$\left[ \text{Cu} \left( \begin{array}{c} \text{S}^b \text{---} \text{C}^d \text{---} \text{S}^f \\ \text{S}^c \text{---} \text{C}^e \text{---} \text{S}^g \\ \text{S}^h \text{---} \text{C}^i \text{---} \text{CH}_3 \\ \text{S}^h \text{---} \text{C}^i \text{---} \text{CH}_3/2 \end{array} \right) \right]^{n=2^- \text{ or } 0}$$

bond	$n = 2^-$	$n = 0$	$\Delta$
<i>a</i>	2.287(1)	2.282(1)	−5
<i>b</i>	1.738(3)	1.683(4)	−55
<i>c</i>	1.341(4)	1.414(9)	73
<i>d</i>	1.766(3)	1.743(4)	−23
<i>e</i>	1.756(3)	1.738(4)	−18
<i>f</i>	1.342(5)	1.361(7)	19
<i>g</i>	1.758(3)	1.737(4)	−21
<i>h</i>	1.748(3)	1.762(4)	14
<i>i</i>	1.330(5)	1.353(9)	23

$[\text{Cu}(\text{dmdt})_2]$  were measured by using a SQUID magnetometer. A Curie–Weiss behavior was observed for  $(^n\text{Bu}_4\text{N})_2[\text{Cu}(\text{dmdt})_2]$  ( $\chi_{\text{rt}} = 1.33 \times 10^{-3} \text{ emu mol}^{-1}$ ,  $C = 0.40 \text{ K emu mol}^{-1}$ ,  $\theta = -0.2 \text{ K}$ ), indicating the existence of an isolated  $S = 1/2$  spin on each molecule. The temperature dependence of the susceptibility of  $[\text{Cu}(\text{dmdt})_2]$  was also completely fitted by a Curie–Weiss plot ( $\chi_{\text{rt}} = 1.09 \times 10^{-3} \text{ emu mol}^{-1}$ ,  $C = 0.33 \text{ emu K mol}^{-1}$ ,  $\theta = -4.2 \text{ K}$ ). The Curie constant suggests the existence of 84% of  $S = 1/2$  spin moments (estimated on the basis of a  $g$  value (2.035) obtained by ESR (electron spin resonance) experiments). These results are inconsistent with the previous reports of the other copper complexes, in which most of the magnetic moments were lost by oxidation to the neutral state. As briefly mentioned before, the bond lengths of the neutral molecule ( $[\text{Cu}(\text{dmdt})_2]$ ) show a considerable difference from those of the dianion in  $(^n\text{Bu}_4\text{N})_2[\text{Cu}(\text{dmdt})_2]$  (Table 4). The schematic drawing of the HOMO and LUMO of  $[\text{Cu}(\text{dmdt})_2]$  is given in Figure 3c. Table 4 shows that by the oxidation from  $[\text{Cu}(\text{dmdt})_2]^{2-}$  to  $[\text{Cu}(\text{dmdt})_2]^0$  all the  $\text{C}=\text{C}$  bonds become longer, indicating that the LUMO has bonding character on each  $\text{C}=\text{C}$  bond. On the other hand, except for bond *h* showing a very small positive change,  $\text{S}-\text{C}$  bonds tend to be shortened, suggesting antibonding character of the LUMO on  $\text{C}-\text{S}$  bonds. Very large changes in bonds *b* and *c* suggest the large amplitude of the LUMO on the S and C atoms in the central five-membered ring. These features are in good agreement with the general features of the calculated molecular orbitals and also those of extended-TTF ligand complexes such as  $[\text{Ni}(\text{ptdt})_2]^{0+}$  and  $[\text{Ni}(\text{tmdt})_2]^{0+}$ .<sup>24,25,28</sup> In other words, the molecular orbital symmetry on the extended-TTF ligands is similar to that of the HOMO of the TTF-like molecule, as expected.<sup>28</sup> The small change of  $\text{Cu}-\text{S}$  bond length and the large change in extended-TTF ligands indicate that the oxidation of  $[\text{Cu}(\text{dmdt})_2]^{2-}$  takes place mainly in the ligand portion.

### 3.2. Metallic Crystal of $[\text{Co}(\text{dt})_2]_2$ with a Dimeric Conformation

As mentioned before, a single-component cobalt complex can be expected to be a magnetic conductor. We synthesized a single-component cobalt complex with tetrathiafulvalenedithiolate ligands.<sup>52</sup> Since the

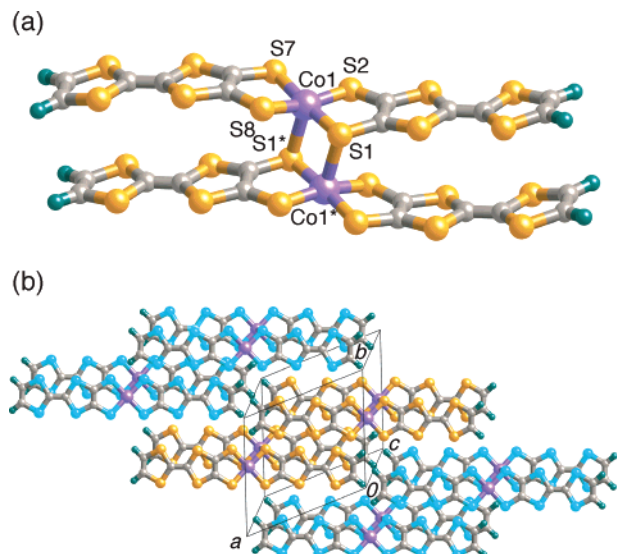


**Figure 24.** (a) Molecular structure of  $[\text{Co}(\text{dt})_2]_2$ . (b) Crystal structure of  $[\text{Co}(\text{dt})_2]_2$ . The cobalt atom has a distorted square pyramidal geometry. A unit cell contains only one  $[\text{Co}(\text{dt})_2]_2$  dimeric molecule, which is surrounded by six  $[\text{Co}(\text{dt})_2]_2$  molecules.

crystals were very small, the synchrotron radiation X-ray powder diffraction experiment of this complex was performed. The imaging plate detectors and the large Debye–Scherrer camera at the facility Spring-8 BL02B2 were used. The structure was solved by the genetic algorithm (GA)<sup>53</sup> and refined by the MEM/Rietveld method, which is a self-consistent iterative analysis of a combination of the maximum entropy method (MEM) and Rietveld analysis.<sup>54</sup> This is the novel metal complex whose structure was determined by a powder diffraction experiment. The crystal data for  $[\text{Co}(\text{dt})_2]_2$  (dt = tetrathiafulvalenedithiolate) are as follows: triclinic,  $P\bar{1}$ ,  $a = 11.7185(3)$  Å,  $b = 10.9513(2)$  Å,  $c = 7.7336(1)$  Å,  $\alpha = 79.737(2)^\circ$ ,  $\beta = 96.474(2)^\circ$ ,  $\gamma = 113.973(2)^\circ$ ,  $V = 891.45(7)$  Å<sup>3</sup>,  $Z = 1$ ,  $R_{wp} = 0.053$ , and  $R_I = 0.082$ .  $[\text{Co}(\text{dt})_2]_2$  is a dimeric molecule (Figure 24a). The cobalt atom has a slightly distorted square pyramidal geometry. The Co–S distances in a plane are 2.166–2.186 Å, and the Co–S distance connecting two monomer units is 2.425 Å. The Co–S–Co angle is almost 89.1°. The long ligands of  $\text{Co}(\text{dt})_2$  are slightly distorted in opposite directions, and each  $\text{Co}(\text{dt})_2$  within a dimeric molecule is parallel to the others. A unit cell contains only one  $[\text{Co}(\text{dt})_2]_2$  dimeric molecule (Figure 24b). The  $[\text{Co}(\text{dt})_2]_2$  dimeric molecule is surrounded by six dimeric molecules along the molecular plane.

Resistivity measurements were made by the four-probe method from room temperature down to 0.6 K on a compaction pellet sample. The room-temperature conductivity of  $[\text{Co}(\text{dt})_2]_2$  is 19 S cm<sup>-1</sup>, a comparatively high conductivity despite the measurement on the compressed pellet sample. The conductivity at 0.55 K is about  $1/10$  of that at room temperature. The magnetic susceptibility at room temperature is  $3.5 \times 10^{-4}$  emu mol<sup>-1</sup>, and it is almost constant above 50 K. 1.6% spins are considered to remain, if Co is in the  $3/2$  high spin state. These data indicate that  $[\text{Co}(\text{dt})_2]_2$  is essentially metallic, at least above 50 K. Simple extended-Hückel tight-binding band calcula-

tions were performed, and 3D electron and hole Fermi surfaces were obtained, which is consistent with the expected metallic properties of  $[\text{Co}(\text{dt})_2]_2$ . Thus,  $[\text{Co}(\text{dt})_2]_2$  is a novel Co complex, where dimeric molecules form a metallic crystal without localized spins.

### 3.3. Single-Component Antiferromagnetic Molecular Metal, $[\text{Au}(\text{tmdt})_2]$ , with $T_N$ around 100 K

Unlike the neutral bis(dithiolato)nickel complex, the neutral bis(dithiolato)gold complex has an odd number of total electrons. However, similar to the nickel complex, the bis(dithiolato)gold complex is planar. In terms of valence electrons, the neutral bis(dithiolato)gold complex is isoelectronic to the planar bis(dithiolato)nickel monoanionic complex with one unpaired electron per molecule, which makes the electromagnetic properties of the neutral gold complex very attractive. It has been thought that these unpaired electrons or holes in the bis(dithiolato)gold complexes have a possibility to form a metallic band. Some gold complexes were examined on the basis of these ideas. Almeida et al. suggested the metallic state of the crystal of the neutral gold dithiolene complex,  $[\text{Au}(\alpha\text{-tpdt})_2]$  ( $\alpha\text{-tpdt} = 2,3\text{-thiophenedithiolate}$ ).<sup>55</sup> Bjørnholm et al. showed that the crystal of  $[\text{Au}(\text{bdt})_2]$  (bdt = benzene-1,2-dithiolate) consisting of nearly uniform stacks of neutral molecular radicals is a semiconductor with one charge carrier per molecule and exhibits a weak dimerization of the stack at low temperature.<sup>56</sup> Schultz et al. found that, in the insulating crystal of  $[\text{Au}(\text{dddt})_2]$  (dddt = 5,6-dihydro-1,4-dithiin-2,3-dithiolate), the molecules form dimers, as in the case of neutral BEDT-TTF molecules.<sup>57</sup> Recently, Fourmigué et al. prepared  $[\text{Au}(\text{F}_2\text{pdt})_2]$  ( $\text{F}_2\text{pdt} = 6,6\text{-difluoro-6,7-dihydro-5H-[1,4]-dithiepine-2,3-dithiolate}$ ).<sup>58</sup> The strong segregation patterns by formation of a layered structure with fluorine bilayers aroused interest in highly fluorinated molecules by introducing a  $\text{CF}_2$  group on a TTF core.

The structural, electrical, and magnetic properties of the crystals composed of single-component gold complexes with extended-TTF ligands,  $[\text{Au}(\text{dmdt})_2]$  and  $[\text{Au}(\text{tmdt})_2]$ , were examined.<sup>59</sup>

Since the crystals were very small, synchrotron radiation X-ray powder experiments were performed to obtain the structural information of  $[\text{Au}(\text{dmdt})_2]$  and  $[\text{Au}(\text{tmdt})_2]$ . The imaging plate detectors and the Large Debye–Scherrer camera at the facility Spring-8 BL02B2 were used. The wavelength of incident X-rays was 1 Å. The exposure time was 200 min. Although sufficient diffraction patterns could not be obtained on  $[\text{Au}(\text{dmdt})_2]$ , an ideal X-ray powder pattern of  $[\text{Au}(\text{tmdt})_2]$  was obtained in  $0.02^\circ$  steps in  $2\theta$  from  $3.0^\circ$  to  $60.0^\circ$ , which showed the crystal structure of  $[\text{Au}(\text{tmdt})_2]$  to be isostructural to that of the single-component molecular metal  $[\text{Ni}(\text{tmdt})_2]^{0+}$ . The lattice constants of  $[\text{Au}(\text{tmdt})_2]$  were determined as  $a = 6.4129(1)$  Å,  $b = 7.5514(2)$  Å,  $c = 12.1543(3)$  Å,  $\alpha = 90.473(3)^\circ$ ,  $\beta = 96.698(2)^\circ$ ,  $\gamma = 103.008(3)^\circ$ , and  $V = 569.21(2)$  Å<sup>3</sup>. The structure was analyzed by the MEM/Rietveld method.<sup>54</sup> The structure of  $[\text{Au}$



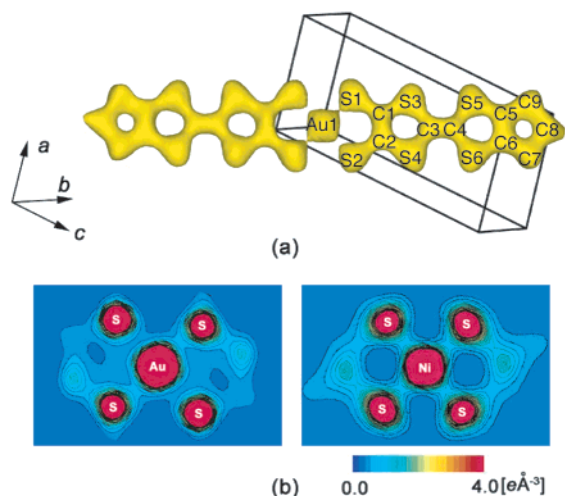


**Figure 25.** (a) Unit lattice and MEM electron density of [Au(tmdt)<sub>2</sub>] as an equi-contour surface of  $1.0 \text{ e } \text{Å}^{-3}$ . (b) Comparison of electron densities of [Au(tmdt)<sub>2</sub>] and [Ni(tmdt)<sub>2</sub>] around the central metal atoms, showing relatively small bonding electron density on Au-S bonds. This depends on the difference of the distribution of d electrons of the central metal atoms.

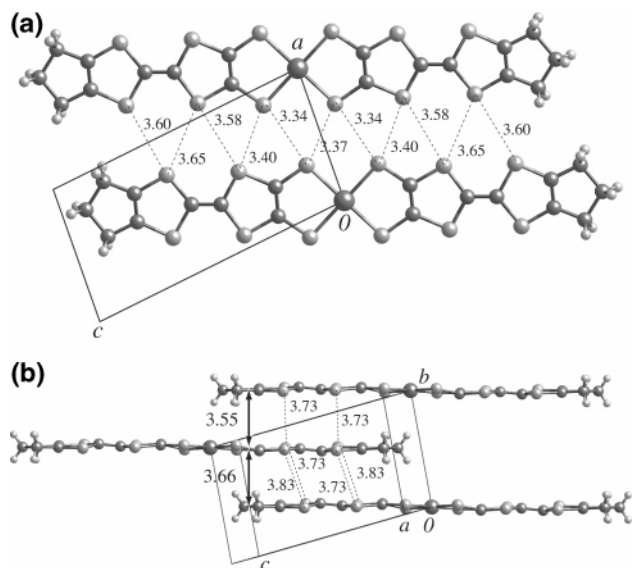


**Figure 26.** (a) Crystal structure viewed along the perpendicular axis of the molecule. (b) Side view of the molecular stacking of [Au(tmdt)<sub>2</sub>]. Intermolecular S...S contacts are a little longer than those found in [Ni(tmdt)<sub>2</sub>]. The average interplanar distance between molecules on (0,0,0) and (1,1,1) is  $3.543 \text{ Å}$ , and that between those on (0,0,0) and (1,0,1) is  $3.667 \text{ Å}$ .

(tmdt)<sub>2</sub>] was successfully visualized as electron densities by using synchrotron radiation powder X-ray diffraction, from which all the atoms were located. The final  $R$  factors for 3751 points (the  $2\theta$  range for analysis is  $2.5 - 40.0^\circ$ ) were  $R_{wp} = 2.8\%$  and  $R_I = 7.3\%$ . Parts a and b, respectively, of Figure 25 show the unit lattice and MEM electron density of [Au(tmdt)<sub>2</sub>] as an equi-contour surface of  $1.0 \text{ e } \text{Å}^{-3}$ . The [Au(tmdt)<sub>2</sub>] molecule is almost planar. The gold atom has a square planar coordination with the average Au-S distance  $2.296(2) \text{ Å}$  and the S-Au-S angle  $89.9(1)^\circ$ . These values well correspond to those of the neutral bis(dithiolato)gold complex [Au(dddt)<sub>2</sub>] (Au-S,  $2.304(5) \text{ Å}$ ; S-Au-S,  $89.15(2)^\circ$ ). The intermolecu-

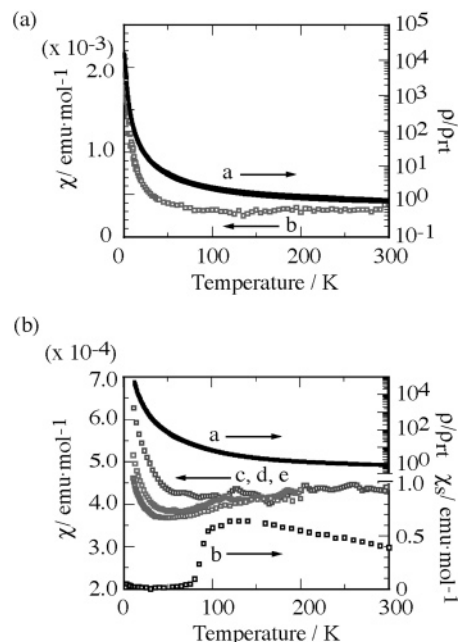


**Figure 27.** (a) Resistivities and susceptibilities of [Au(dmdt)<sub>2</sub>]: (a) Resistivity of a compaction pellet ( $\rho_{RT} = 0.083 \text{ } \Omega \text{ cm}$ , activation energy =  $9 \text{ meV}$ ). (b) Magnetic susceptibility measured at  $30 \text{ kOe}$ . Magnetic susceptibility of  $3.4 \times 10^{-4} \text{ emu mol}^{-1}$  at room temperature and Pauli-like paramagnetism above  $50 \text{ K}$ . (b) Resistivities and susceptibilities of [Au(tmdt)<sub>2</sub>]: (a) Resistivity of a compaction pellet ( $\rho_{RT} = 0.067 \text{ } \Omega \text{ cm}$ ). These data indicate that [Au(dmdt)<sub>2</sub>] is essentially metallic at least above  $50 \text{ K}$ . (b) Spin susceptibility by ESR of polycrystalline samples: spin susceptibility at room temperature =  $3.8 \times 10^{-4} \text{ emu mol}^{-1}$ ,  $\Delta H_{pp} = 250 \text{ G}$ , and  $g = 2.005$ . (c-e) Magnetic susceptibilities by SQUID at  $30$  (c <  $300 \text{ K}$ ),  $10$  (d <  $200 \text{ K}$ ), and  $3$  (e <  $200 \text{ K}$ ) kOe. No anomaly at  $30 \text{ kOe}$  and the susceptibility decrease around  $100 \text{ K}$  below  $10 \text{ kOe}$  seem to suggest the possibility that the  $100 \text{ K}$  transition is an antiferromagnetic transition with the critical magnetic field of the spin flipping transition between  $10$  and  $30 \text{ kOe}$ .

lar S...S contacts less than the sum of the van der Waals radii ( $3.43\text{--}3.64 \text{ Å}$ ) are a little longer than those found in [Ni(tmdt)<sub>2</sub>] (Figure 26a). The average interplanar distance between the molecules on (0,0,0) and (1,1,1) is  $3.543 \text{ Å}$  and that between those on (0,0,0) and (1,0,1) is  $3.667 \text{ Å}$  (Figure 26b).

The resistivity measurements were made by the four-probe method from room temperature down to  $0.6 \text{ K}$  on a compaction pellet sample of [Au(dmdt)<sub>2</sub>], which gave a fairly large room-temperature conductivity of  $9 \text{ meV}$  ( $50\text{--}300 \text{ K}$ ) (Figure 27a). The magnetic susceptibilities of [Au(dmdt)<sub>2</sub>] were measured with a SQUID magnetometer at  $30 \text{ kOe}$  in the temperature range from  $300$  to  $1.9 \text{ K}$  (Figure 27a). The data were corrected for the diamagnetic contribution ( $\chi^{\text{dia}} = -3.25 \times 10^{-4} \text{ emu mol}^{-1}$ ). The magnetic susceptibility was  $3.4 \times 10^{-4} \text{ emu mol}^{-1}$  at room temperature and showed Pauli-like paramagnetism at least above  $50 \text{ K}$ , which is consistent with the results of ESR measurements. Despite the weakly semiconducting behavior of the compaction sample, these data indicate that [Au(dmdt)<sub>2</sub>] is essentially metallic at least above  $50 \text{ K}$ .

The compaction pellet sample of [Au(tmdt)<sub>2</sub>] also showed a large room-temperature conductivity of  $15$

$\text{S cm}^{-1}$  and a small activation energy of 20 meV (50–300 K) (Figure 27b). The XPS (X-ray photoelectron spectroscopy) and NEXAFS (near edge X-ray absorption fine structure) measurements suggested the valence of the central metal of the neutral gold complex  $[\text{Au}(\text{tmdt})_2]$  to be almost the same as that in  $[\text{Au}(\text{tmdt})_2]^-$  and the existence of DOS at the Fermi level, indicating the system to be a metal.<sup>60</sup> ESR spectra of polycrystalline samples of  $[\text{Au}(\text{tmdt})_2]$  were measured in the temperature range 3.5–300 K (Figure 27b). The spin susceptibility, peak-to-peak line width, and  $g$  value at room temperature were  $\chi_s = 3.8 \times 10^{-4} \text{ emu mol}^{-1}$ ,  $\Delta H_{\text{pp}} = 250 \text{ G}$ , and  $g = 2.005$ . As shown in Figure 27b, the  $\chi_s$  values increased gradually down to 130 K and decreased abruptly at 100 K, where an onset of a rapid increase of the line width was observed. These facts indicate that  $[\text{Au}(\text{tmdt})_2]$  undergoes a magnetic transition around 100 K while keeping its high conducting state. The magnetic susceptibility of a polycrystalline sample of  $[\text{Au}(\text{tmdt})_2]$  was measured with the SQUID magnetometer under magnetic fields of 30, 10, 5, and 3 kOe. As seen from Figure 27b, for magnetic fields above 30 kOe, the susceptibilities were roughly constant above 50 K, below which the magnetic impurities seemed to dominate the susceptibility behavior. Unlike the gradual increase of  $\chi_s$ , the magnetic susceptibilities were approximately constant down to 100 K even at 3 kOe, indicating the temperature dependence of  $\chi_s$  to be possibly affected by the skin effect of microwave. Around 100 K the susceptibility decrease indicating the magnetic transition was observed, which was consistent with the ESR behavior. To our knowledge, there has been no molecular conductor exhibiting an (antiferro)magnetic transition at temperatures as high as 100 K without loss of its high conductivity. But no anomaly above 30 kOe and the susceptibility decrease around 100 K below 10 kOe seem to suggest the possibility that the 100 K transition was an antiferromagnetic transition with the critical magnetic field of the spin flipping transition between 10 and 30 kOe. Very recently the first principle band structure calculation was performed by Ishibashi et al.<sup>61</sup> This calculation suggested that the Fermi surface of  $[\text{Au}(\text{tmdt})_2]$  contains warped Fermi surfaces, which can be nested, and that a small Fermi surface still remains below 100 K, which retains the system as highly conducting even at low temperature.  $^1\text{H NMR}$  studies of  $[\text{Au}(\text{tmdt})_2]$  by Kanoda et al. also revealed that the phase transition that occurred around 85 K is the antiferromagnetic phase transition.<sup>62</sup> The synchrotron X-ray powder diffraction experiments from room temperature down to 20 K showed no extra change of the crystal lattice occurred, which also suggested that the phase transition is the SDW transition.<sup>63</sup>

### 3.4. Single-Component Pd Complexes

To compare the crystal structure and the electronic structure of single component palladium complexes with Ni complexes, we synthesized  $[\text{Pd}(\text{dt})_2]$ <sup>64</sup> and  $[\text{Pd}(\text{C3-tdt})_2]$  (C3-tdt = di-*n*-propylthiotetrathiafulvalenedithiolate).<sup>65</sup>

Since the sizes of the obtained crystals were very small, we could not determine the crystal structure

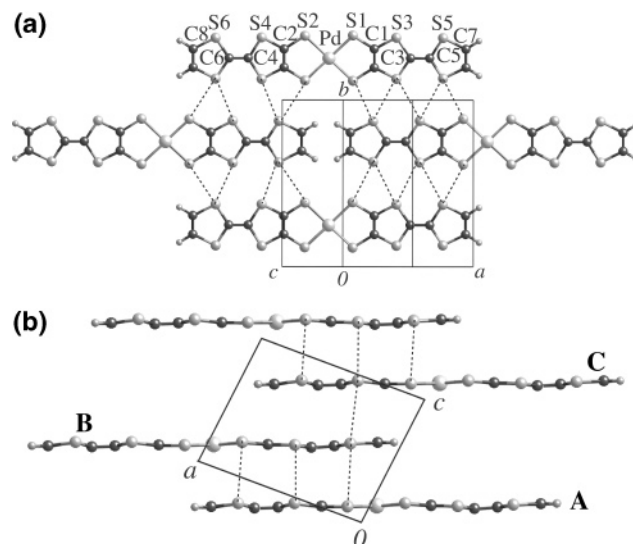


**Figure 28.** Crystal structure of  $[\text{Pd}(\text{dt})_2]$ . The palladium atom has a square planar coordination geometry, and the twelve sulfur atoms on the ligands are coplanar. (a) Arrangement of  $[\text{Pd}(\text{dt})_2]$  viewed perpendicular to the molecular plane. (b) Bridged structure of  $[\text{Pd}(\text{dt})_2]$  viewed along the  $b$ -axis. One  $\text{Pd}(\text{dt})_2$  molecule is adjacent to four molecules in the transverse direction and overlaps with the upper two molecules.

of  $[\text{Pd}(\text{dt})_2]$  by X-ray single-crystal structure analysis. Therefore, the synchrotron radiation X-ray powder diffraction experiment was performed to gain information on the crystal structure. The experiment was carried out by the imaging plate detectors and the Large Debye–Scherrer camera at the facility SPring-8 BL02B2. The wavelength of incident X-rays was 1 Å. The exposure time was 200 min. An ideal X-ray powder pattern of  $[\text{Pd}(\text{dt})_2]$  was obtained in  $0.02^\circ$  steps in  $2\theta$  from  $3.0$  to  $60.0^\circ$ .

The crystal structure of  $[\text{Pd}(\text{dt})_2]$  was successfully analyzed by the GA and the MEM/Rietveld methods.<sup>53,54</sup> Similar to the case of the  $[\text{Co}(\text{dt})_2]$  complex, this is a unique example of the structure determination of the powder sample with unknown structure by synchrotron radiation X-ray powder experiments. The final  $R$  factors for 3751 points (the  $2\theta$  range for analysis is  $2.5$ – $40.0^\circ$ ) were  $R_{\text{wp}} = 3.9\%$  and  $R_I = 7.1\%$ , respectively. The lattice constants of  $[\text{Pd}(\text{dt})_2]$  ( $\text{C}_{12}\text{H}_4\text{S}_{12}\text{Pd}$ ) are  $a = 10.0465(2) \text{ \AA}$ ,  $b = 11.5882(2) \text{ \AA}$ ,  $c = 7.9613(3) \text{ \AA}$ ,  $\beta = 96.7677(5)^\circ$ , and  $V = 920.41(2) \text{ \AA}^3$  with space group  $P2_1/m$  and  $Z = 2$ . The crystal structures of  $[\text{Pd}(\text{dt})_2]$  are shown in Figure 28. A palladium atom has the square planar coordination geometry, and twelve sulfur atoms on ligands exist on the coplanarity. The palladium atom and the two C=C bonds (C(3)–C(5) and C(4)–C(6)) on the TTF frame are located on the mirror plane, and half of the  $[\text{Pd}(\text{dt})_2]$  molecule is crystallographically independent. The average Pd–S bond distance and the average S–Pd–S angle are  $2.288(2) \text{ \AA}$  and  $86.5^\circ$ , respectively. As shown in Figure 28a, one  $[\text{Pd}(\text{dt})_2]$  molecule contacts four molecules in the transverse direction and overlaps with the upper two molecules. The molecule is stacked along the  $[100]$  and  $[101]$  directions with slip distances of  $10.046$  and  $13.379 \text{ \AA}$ , respectively. The interplanar distances are  $3.39 \text{ \AA}$  between molecules **A** and **B** and  $3.64 \text{ \AA}$  between

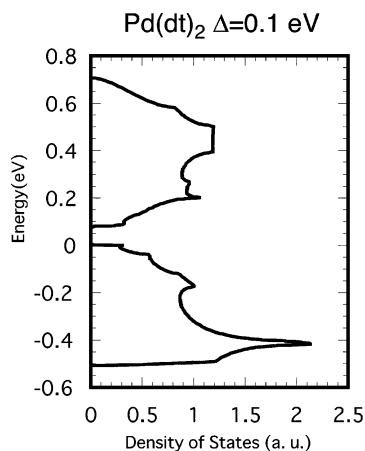


**Figure 29.** Density of state of  $[\text{Pd}(\text{dt})_2]$ . The HOMO–LUMO gap is assumed as 0.1 eV. The calculations suggest that the semiconducting state exists when  $\Delta E < 0.2$  eV. The semiconducting behavior of  $[\text{Pd}(\text{dt})_2]$  is consistent with the result of the tight-binding band structure calculation, suggesting large HOMO–LUMO interactions.

molecules **B** and **C**. The Pd···Pd distances are 13.532 Å for **A** and **B**, and 10.046 Å for **B** and **C** (Figure 28b). As illustrated in Figure 28a, there are many intermolecular S···S contacts less than the sum of van der Waals radii along the transverse direction and in the direction of  $[100]$  and  $[10\bar{1}]$ .

The electrical resistivity of the compressed pellet sample of  $[\text{Pd}(\text{dt})_2]$  was measured by a usual four-probe method down to 50 K, which showed the semiconducting behavior with the room-temperature conductivity of  $0.3 \text{ S cm}^{-1}$  and the activation energy of 94 meV.

The extended-Hückel tight-binding band structure calculation of  $[\text{Pd}(\text{dt})_2]$  was carried out by use of Slater-type atomic orbitals. Schematic drawings of the HOMO and LUMO orbitals of  $[\text{Pd}(\text{dt})_2]$  are shown in Figure 3c. The molecule of  $[\text{Pd}(\text{dt})_2]$  has approximately  $D_{2h}$  symmetry. As expected, the HOMO has  $b_{1u}$  symmetry and has the same sign on every chalcogen atom. On the other hand, the symmetry of the LUMO is  $b_{2g}$ , and it has the nodal plane on the central palladium atom. The obtained DOS is shown in Figure 29. The band structure calculations were performed with changing HOMO–LUMO gap at  $0 < \Delta E < 1.0$  eV. It is interesting that the semiconducting state was suggested for  $\Delta E < 0.2$  eV but the weakly metallic state was suggested for  $\Delta E > 0.25$  eV. At first sight, these results seem to show that the extremely small HOMO–LUMO gap, which has been considered to be the most essential requirement for the realization of highly conducting single-component molecular systems, is not a dominant factor to produce the Fermi surfaces in this complex. But the existence of a band gap for  $\Delta E > 0.2$  eV is consistent with the large HOMO–LUMO interaction being comparable to the HOMO–HOMO and LUMO–LUMO interactions, which tends to produce the energy gap, especially when  $\Delta E$  is small. Two large peaks of the DOS separated by about 0.85 eV (Figure 29) are consistent with the broad maximum of the electronic absorption spectra of  $[\text{Pd}(\text{dt})_2]$  around 1 eV, which is described in section 4.<sup>66</sup> The semiconducting

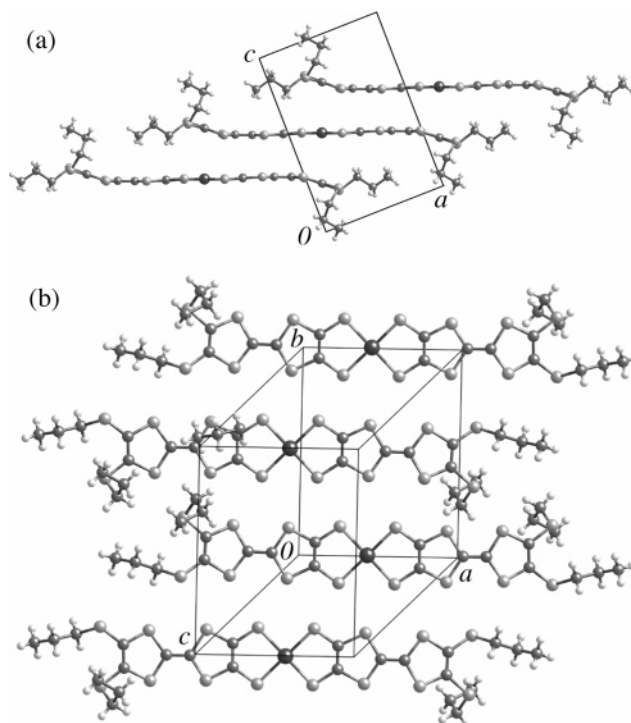


**Figure 30.** Crystal structure of  $[\text{Pd}(\text{C3-tdt})_2]$  projected onto (a) the  $ac$ -plane and (b) the  $bc$ -plane. The molecular structure is almost planar except for four  $n$ -propylthio groups, and it is more planar than that of the monoanion  $[\text{Pd}(\text{C3-tdt})_2]^-$ . The complexes are stacked along the  $a$  direction. Crystal data of  $[\text{Pd}(\text{C3-tdt})_2]$ :  $\text{C}_{24}\text{H}_{28}\text{S}_{16}\text{Pd}$ , triclinic,  $P\bar{1}$ ,  $a = 10.007(7)$  Å,  $b = 12.019(9)$  Å,  $c = 15.92(1)$  Å,  $\alpha = 112.14(1)^\circ$ ,  $\beta = 89.665(6)^\circ$ ,  $\gamma = 90.02(1)^\circ$ ,  $Z = 2$ ,  $V = 1773(2)$  Å<sup>3</sup>.

properties of  $[\text{Pd}(\text{dt})_2]$  suggest  $\Delta E$  to be less than 0.2 eV.

$[\text{Pd}(\text{C3-tdt})_2]$  with bulky  $n$ -propylthio groups in the terminal site is less conducting ( $\sigma(\text{RT}) = 10^{-2} \text{ S cm}^{-1}$ ). The crystal structure of  $[\text{Pd}(\text{C3-tdt})_2]$  is shown in Figure 30.<sup>65</sup>

#### 4. Infrared Electronic Absorption in Single-Component Molecular Metals

It is commonly accepted that the electronic energy of a molecule is much higher than the vibrational energy of a molecule. For example, the energy of the longest-wavelength electronic absorption of a typical  $\pi$  molecule, anthracene (3.4 eV), is much larger than the vibrational energy of a hydrogen molecule ( $4400 \text{ cm}^{-1}$  0.55 eV), namely, the highest energy of molecular vibration. If a molecule with electronic excitation in the infrared (IR) region can be designed, then the molecular system is expected to have unprecedented electronic properties. To develop a metallic crystal consisting of single-component molecules, we have synthesized molecules with unprecedentedly low electronic excitation (or an unprecedentedly small HOMO–LUMO gap).<sup>66</sup>

In general, the simplest “1D box model” of  $\pi$ -conjugated molecules predicts that the wavelength of the longest wavelength electronic absorption ( $\lambda_{\text{max}}$ ) will become longer as the size of the  $\pi$  molecule increases. However, synthesizing molecules with very long  $\pi$  systems is not trivial because of synthetic inacces-

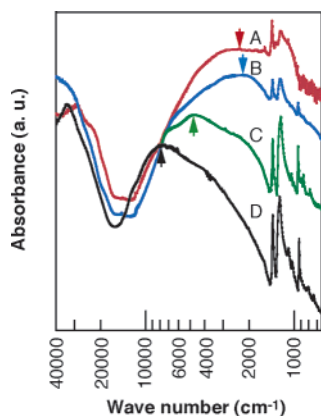


**Figure 31.** Visible and IR spectra of (A) [Ni(tmdt)<sub>2</sub>] (400 S cm<sup>-1</sup>), [Ni(dmdt)<sub>2</sub>] (350 S cm<sup>-1</sup>), [Ni(ptdt)<sub>2</sub>] (7 S cm<sup>-1</sup>), and [Pd(dt)<sub>2</sub>] (0.3 S cm<sup>-1</sup>). The room-temperature conductivities are in parentheses. The vis and IR spectra connected smoothly around 6000 cm<sup>-1</sup>. The broad absorption maximum (arrow) shifts to higher energy from 2200 to 7800 cm<sup>-1</sup> as the semiconducting properties are increased.

sibility, chemical instability, and poor solubility.<sup>67</sup> Fused porphyrin is an example of molecules with small electronic excitation energies. The absorption maximum of fused porphyrin was observed at about 1250 nm (1.0 eV), and the absorption showed a strong red shift with increasing numbers of fused porphyrins.<sup>68</sup> It will be extremely difficult to prepare a fully  $\pi$  conjugated porphyrin oligomer longer than an icosamer ( $n > 20$ ) without the effective conjugated length (ECL) effect,<sup>69</sup> which is also expected to show a similar low-energy electronic excitation. Nevertheless, Tsuda and Osuka succeeded in preparing fully conjugated linear porphyrin oligomers with electronic absorption bands that reach into the IR region, and  $\lambda_{\max}^{-1}$  decreased as the number of porphyrins ( $n$ ) increased and that for  $n = 12$  (dodecamer) was about 3500 cm<sup>-1</sup> (0.45 eV).<sup>67</sup> Another example of a small HOMO–LUMO gap (0.6 eV) is that for aromatic heterocycles and a novel nonclassical thiophene with pyrazine–dihydropyrazine whose lowest-energy absorption edge was observed at about 2100 nm.<sup>70</sup> Two polymers of *syn*-naphthodithiophenes (NDT) and *anti*-NDT have very low band gaps of  $\sim 0.8$  eV.<sup>71</sup> On the other hand, the most straightforward way to engineer a small HOMO–LUMO gap is to design a molecule that incorporates covalently linked donor and acceptor moieties. It has been reported that a TTF–fluorene conjugate possesses the smallest HOMO–LUMO gap (0.3 eV) for closed-shell organic compounds and exhibits an intramolecular charge-transfer band around 8000 cm<sup>-1</sup>.<sup>72</sup>

We have synthesized and examined the electronic absorption spectra of a transition metal complex with extended-TTF dithiolate ligands [M(L)<sub>2</sub>] [M = Ni, Pd; L = tmdt, dmdt, ptdt, and dt]. Since these complexes are not soluble in the usual organic solvent, the visible (vis) and IR spectra were measured on crystalline powder samples. Figure 31 shows the IR spectra have molecular vibration peaks and broad electronic absorption. [Ni(tmdt)<sub>2</sub>] and [Ni(dmdt)<sub>2</sub>] exhibited the broadest absorption maxima around 2200 cm<sup>-1</sup> ( $\lambda_{\max}^{-1}$ ), which is much smaller than the wavenumber for the porphyrine dodecamer ( $n = 12$ ,

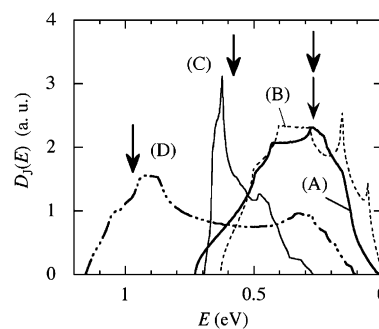


**Figure 32.** Calculated joint density of states  $D_j(E)$  for (A) [Ni(tmdt)<sub>2</sub>], (B) [Ni(dmdt)<sub>2</sub>], (C) [Ni(ptdt)<sub>2</sub>], and (D) [Pd(dt)<sub>2</sub>]. The  $E$ -dependence of  $D_j(E)$  is consistent with the observed electronic absorption spectra for each system. The arrows indicate the energies of observed absorption maxima ( $\lambda_{\max}^{-1}$ ).

$\lambda_{\max}^{-1} \approx 3500$  cm<sup>-1</sup>). So far as we know, this is the smallest electronic absorption energy ever reported for single-component molecular systems. On the other hand, semiconducting complexes, [Ni(ptdt)<sub>2</sub>] and [Pd(dt)<sub>2</sub>], exhibited absorption maxima at 4700 and 7800 cm<sup>-1</sup>, respectively.

The electronic absorbance is considered to be proportional to  $D_j \mu^2$ , where  $D_j$  is the joint density of state and  $\mu$  is the transition dipole. We could show that the  $E$ -dependence of  $D_j(E)$  can be regarded as the calculated electronic spectrum. As shown in Figure 32, the calculated absorption maximum was around 0.3 eV for [Ni(tmdt)<sub>2</sub>] and [Ni(dmdt)<sub>2</sub>], around 0.6 eV for [Ni(ptdt)<sub>2</sub>], and around 0.9 eV for [Pd(dt)<sub>2</sub>], which are consistent with the wavenumbers of the observed absorption maxima:  $\lambda_{\max}^{-1} = 2200$  cm<sup>-1</sup> (0.27 eV) for [Ni(tmdt)<sub>2</sub>] and [Ni(dmdt)<sub>2</sub>], 4700 cm<sup>-1</sup> (0.58 eV) for [Ni(ptdt)<sub>2</sub>], and 7800 cm<sup>-1</sup> (0.97 eV) for [Pd(dt)<sub>2</sub>]. These facts show that the single-component molecular conductors are composed of the molecules with an unprecedentedly small HOMO–LUMO gap. Although the electronic absorptions around 2200 cm<sup>-1</sup> of [Ni(tmdt)<sub>2</sub>] and [Ni(dmdt)<sub>2</sub>] seem to suggest an extremely small HOMO–LUMO gap ( $\Delta E$ ), the [M(L)<sub>2</sub>] peaks blue shifted as the semiconducting properties of the crystal increased, which indicates that the band structure plays a crucial role.

The bonding and antibonding combinations of the left and right ligand orbitals, respectively ( $\phi_{\text{HOMO}} \approx \phi_{\text{ligand1}} + \phi_{\text{ligand2}}$ ;  $\phi_{\text{LUMO}} \approx \phi_{\text{ligand1}} - \phi_{\text{ligand2}} + c_{\text{M}} \phi_{\text{d}\pi}$ , where  $c_{\text{M}} \phi_{\text{d}\pi}$  is the small contribution from the  $\text{d}\pi$  orbital of the central metal atom), can approximate the HOMO and LUMO of a [M(L)<sub>2</sub>] (M = Ni, Pd, ...; L = extended-TTF ligand) molecule.<sup>28</sup> The wave function of the tight-binding band in Ni(L)<sub>2</sub> (L = tmdt, dmdt) crystals, which have one molecule in the unit cell, can be written as  $\Phi(k) = (1/N)^{1/2} [\sum \exp(ikR_n) \{c_{\text{HOMO}}(k) \phi_{\text{HOMO}}(r-R_n) + c_{\text{LUMO}}(k) \phi_{\text{LUMO}}(r-R_n)\}]$ , and the transition dipole  $\mu$  between  $\Phi_{\text{occ}}(k)$  and  $\Phi_{\text{vac}}(k)$  is  $(c_{\text{vac}^*}^{\text{HOMO}}(k) c_{\text{occ}}^{\text{LUMO}}(k) + c_{\text{vac}^*}^{\text{LUMO}}(k) c_{\text{occ}}^{\text{HOMO}}(k)) \mu_{\text{HL}}$ , where  $\mu_{\text{HL}}$  is  $\langle \phi_{\text{LUMO}} | r | \phi_{\text{HOMO}} \rangle$ . Although a substantial HOMO–LUMO mixing in several parts of the Brillouin zone was suggested by Rovira et al.,<sup>47</sup> the HOMO–LUMO mixing around the energy where the DOS has a large value was tentatively assumed to be not so serious due to the crossing-band nature of the Ni(L)<sub>2</sub> system. Then,  $\mu \approx \mu_{\text{HL}}$  and the absorbance

is approximately proportional to  $D_j(E) (= \sum_k (D^{\text{occ}}(k, \epsilon(k)) D^{\text{vac}}(k, \epsilon(k) + E))$ , when  $\epsilon_F - E < \epsilon(k) < \epsilon_F$  ( $\epsilon_F =$  Fermi energy). Thus, the  $E$ -dependence of  $D_j(E)$  can be roughly regarded as the calculated electronic spectrum.

Since it is difficult to accurately estimate the  $\Delta E$ , the extended-Hückel tight-binding band structures and the  $D_j(E)$  of  $[M(L)_2]$  were calculated by varying  $\Delta E$  at  $\Delta E < 1.0$  eV. The calculated spectra agreed with the observed spectra when  $\Delta E = 0.14 \pm 0.06$  eV for  $[\text{Ni}(\text{L})_2]$  and  $0.12 \pm 0.08$  eV for  $[\text{Pd}(\text{dt})_2]$ . Very recently, Ishibashi has evaluated  $D_j(E)$  of  $[\text{Ni}(\text{tmtd})_2]$  on the basis of the local density approximation (LDA) band structure calculation using the *ab initio* plane-wave norm-conserved pseudopotential method, which gave essentially the same spectra around the absorption maximum.<sup>73</sup> That is,  $\Delta E$  seems to be less than  $\sim 0.2$  eV. It should be noted that  $\lambda_{\text{max}}^{-1}$  does not correspond directly to the HOMO–LUMO gap ( $\Delta E$ ).

Thus, the general feature of the IR electronic spectra of  $[M(L)_2]$ , especially the blue shift of the IR electronic absorption spectra, is well explained by the calculated  $D_j(E)$ . It may be said that the recent developments in single-component molecular metals were realized by successfully designing molecules with unprecedentedly small HOMO–LUMO gaps.

## 5. Conclusions and Future Prospects

We presented the basic idea for the design of a single-component molecular metal. The crucial step is the development of a molecule with a small HOMO–LUMO gap and a TTF skeleton. Needless to say, in the  $\pi$  conjugated system, the HOMO–LUMO gap can be reduced by extending the  $\pi$  systems. However, we have proposed a new idea to reduce the HOMO–LUMO gap, which will be useful in future studies on the bottom-up construction of new functional molecular systems because the properties of the molecular system are mainly governed by the nature of the frontier orbitals. The syntheses, the structure analyses, and the physical properties of various single-component molecular conductors, including the first single-component molecular metal,  $[\text{Ni}(\text{tmtd})_2]$ , were also presented. The discovery of a single-component molecular metal has removed the boundary of molecular crystals and metallic crystals, which will provide various possibilities for future studies on the development of new functional molecular systems.

## 6. Acknowledgments

The authors are thankful to Drs. H. Tanaka, M. Kumasaki, and W. Suzuki, Mr. Okano, and Dr. H. Fujiwara for syntheses and characterizations of single-component molecular conductors. The authors are also thankful to Profs. M. Sakata and M. Takada and Dr. E. Nishibori and Mr. Y. Fujishiro for X-ray powder diffraction and Dr. Kato for synchrotron radiation experiments at Spring-8 BL02B2, Dr. M. Tokumoto and Prof. J. Brooks for dHvA oscillation studies at very high magnetic field, Dr. Ishibashi and Prof. K. Terakura for first principle band structure calculations, Prof. Kanoda and Dr. Miyagawa and

Mr. Y. Hara for  $^1\text{H}$  NMR, and Dr. H. Kondo and Prof. T. Ohta for XPS and NAXAFS measurements. The authors are especially thankful to Prof. H. Fukuyama for valuable discussions and continuous encouragement. This study was partly supported by a Grant-in-aid for Scientific Research on (S) (No. 14103005) Priority Areas of Molecular Conductors (No. 15073209) and by the 21st Century COE Program for Frontiers in Fundamental Chemistry from the Ministry of Education, Culture, Sports, Science and Technology. This work was also supported by CREST (Core Research for Evolutional Science and Technology of JST (Japan Science and Technology Corporation)).

## 7. References

- (1) (a) Comès, R.; Lambert, M.; Launois, H.; Zeller, H. R. *Phys. Rev.* **1973**, *B8*, 571. (b) Renker, B.; Pintchovius, L.; Glaser, W.; Rietschel, H.; Comès, R.; Liebert, L.; Drexel, W. *Phys. Rev. Lett.* **1974**, *32*, 836. (c) Deiseroth, H. J.; Shultz, H. *Phys. Rev. Lett.* **1974**, *33*, 963.
- (2) (a) Krogmann, K.; Hausen, H. D. *Z. Anorg. Allg. Chem.* **1968**, *358*, 67. (b) Krogmann, K. *Angew. Chem., Int. Ed.* **1969**, *8*, 35.
- (3) Thielemans, M.; Deltour, R.; Jérôme, D.; Cooper, J. R. *Solid State Commun.* **1976**, *19*, 21.
- (4) (a) Ferraris, J. P.; Cowan, D. O.; Walatka, V., Jr.; Perlstein, J. H. *J. Am. Chem. Soc.* **1973**, *95*, 948. (b) Keller, H. J. *Chemistry and Physics of One-dimensional Metals*; NATO ASI Series B; 1977; Volume 25.
- (5) Jérôme, D.; Mazaud, M.; Ribault, M.; Bechgaard, K. *J. Phys. Lett.* **1980**, *41*, L95.
- (6) Jérôme, D. *Science* **1991**, *252*, 1509.
- (7) Mori, T.; Kobayashi, A.; Sasaki, Y.; Kobayashi, H.; Saito, G.; Inokuchi, H. *Bull. Chem. Soc. Jpn.* **1984**, *57*, 627.
- (8) Thorup, N.; Rindorf, G.; Soling, H.; Bechgaard, K. *Acta Crystallogr.* **1981**, *B37*, 1236.
- (9) Yagubskii, E. B.; Shchegolev, I. F.; Laukhin, V. N.; Kononovich, P. A.; Kartsovnik, M. V.; Zvarykina, A. V.; Buravov, L. I. *JETP Lett.* **1984**, *39*, 12.
- (10) Kobayashi, A.; Kato, R.; Kobayashi, H.; Moriyama, S.; Nishio, Y.; Kajita, K.; Sasaki, W. *Chem. Lett.* **1987**, 459.
- (11) Williams, J. M.; Ferraro, J. R.; Thorn, R. J.; Carlson, K. D.; Geiser, U.; Wang, H. H.; Kini, A. M.; Whangbo, M.-H. *Organic Superconductors (Including Fullerenes)*; Prentice Hall: Englewood Cliffs, NJ, 1992.
- (12) (a) Underhill, A. E.; Ahmad, M. M. *J. Chem. Soc., Chem. Commun.* **1981**, 67. (b) Kobayashi, A.; Mori, T.; Sasaki, Y.; Kobayashi, H.; Ahmad, M. M.; Underhill, A. E. *J. Chem. Soc., Chem. Commun.* **1982**, 390.
- (13) (a) Brossard, L.; Ribault, M.; Valade, L.; Cassoux, P. *Physica B & C (Amsterdam)* **1986**, *143*, 378. (b) Cassoux, P.; Valade, L.; Kobayashi, H.; Kobayashi, A.; Clark, R. A.; Underhill, A. E. *Coord. Chem. Rev.* **1991**, *110*, 115.
- (14) Kobayashi, A.; Kim, H.; Sasaki, Y.; Kato, R.; Kobayashi, H. *Solid State Commun.* **1987**, *62*, 57.
- (15) (a) Canadell, E.; Rachidi, E. I.; Ravy, S.; Pouget, J.-P.; Brossard, L.; Legros, J.-P. *J. Phys. (Paris)* **1989**, *50*, 2967. (b) Canadell, E.; Ravy, S.; Pouget, J.-P.; Brossard, L. *Solid State Commun.* **1990**, *75*, 633.
- (16) Kurmoo, M.; Graham, A. W.; Day, P.; Coles, S. J.; Hursthouse, M. B.; Caulfield, J. L.; Singleton, J.; Pratt, F. L.; Hayes, W.; Ducasse, L.; Guionneau, P. *J. Am. Chem. Soc.* **1995**, *117*, 12209.
- (17) (a) Ojima, E.; Fujiwara, H.; Kato, K.; Kobayashi, H.; Tanaka, H.; Kobayashi, A.; Tokumoto, M.; Cassoux, P. *J. Am. Chem. Soc.* **1999**, *121*, 5581. (b) Fujiwara, H.; Ojima, E.; Nakazawa, Y.; Narymbetov, B. Zh.; Kato, K.; Kobayashi, H.; Kobayashi, A.; Tokumoto, M.; Cassoux, P. *J. Am. Chem. Soc.* **2001**, *123*, 306.
- (18) Coronado, E.; Ggalañ-Mascaros, J.; Gomez-Garcia, C. J.; Laukhin, V. *Nature* **2000**, *408*, 447.
- (19) Eley, D. D. *Nature* **1948**, *162*, 819.
- (20) Akamatu, H.; Inokuchi, H. *J. Chem. Phys.* **1950**, *18*, 810.
- (21) (a) Ito, T.; Shirakawa, H.; Ikeda, S. *J. Polym. Sci., Polym. Chem. Ed.* **1974**, *12*, 11. (b) Shirakawa, H.; Louis, E. J.; MacDiarmid, A. G.; Chiang, C. K.; Heeger, A. J. *J. Chem. Soc., Chem. Commun.* **1977**, 578.
- (22) For example: (a) Barclay, T. M.; Codes, A. W.; de Laat, R. H.; Goddard, J. D.; Haddon, R. C.; Jeter, D. Y.; Mawhinney, R. C.; Oakley, R. T.; Palstra, T. T. M.; Patenaude, G. W.; Reed, R. W.; Westwood, N. P. C. *J. Am. Chem. Soc.* **1997**, *119*, 2633. (b) Itkis, M. E.; Chi, X.; Cordes, A. W.; Haddon, R. C. *Science* **2002**, *296*, 1443.
- (23) Cassoux, P. *Science* **2001**, *291*, 263.

- (24) Tanaka, H.; Okano, Y.; Kobayashi, H.; Suzuki, W.; Kobayashi, A. *Science* **2001**, *291*, 285.
- (25) Kobayashi, A.; Tanaka, H.; Kobayashi, H. *J. Mater. Chem.* **2001**, *11*, 2078.
- (26) Tanaka, H.; Tokumoto, M.; Ishibashi, S.; Okano, Y.; Graf, D.; Choi, E. S.; Brooks, J. S.; Yasuzuka, S.; Kobayashi, H.; Kobayashi, A. *J. Am. Chem. Soc.* In press.
- (27) Canadell, E. *New J. Chem.* **1997**, *21*, 1147.
- (28) Kobayashi, A.; Tanaka, H.; Kumasaki, M.; Torii, H.; Narymbetov, B.; Adachi, T. *J. Am. Chem. Soc.* **1999**, *121*, 10763.
- (29) Arai, E.; Fujiwara, H.; Kobayashi, H.; Kobayashi, A.; Takimiya, K.; Otsubo, T.; Ogura, F. *Inorg. Chem.* **1998**, *37*, 2850.
- (30) Tanaka, H.; et al. To be published.
- (31) Tanaka, H.; Kobayashi, H.; Kobayashi, A. *J. Am. Chem. Soc.* **2002**, *124*, 10002.
- (32) Kini, A. M.; Tytko, S. E.; Hunt, J. E.; Williams, J. M. *Tetrahedron Lett.* **1987**, *28*, 4153.
- (33) Gonnella, N. C.; Cava, M. P. *J. Org. Chem.* **1978**, *43*, 369.
- (34) Svenstrup, N.; Rasmussen, K. M.; Hansen, T. K.; Becher, J. *Synthesis* **1994**, 809.
- (35) Corey, E. J.; Märkl, G. *Tetrahedron Lett.* **1967**, *33*, 3201.
- (36) Miles, M. G.; Wagner, J. S.; Wilson, J. D.; Siedle, A. R. *J. Org. Chem.* **1975**, *40*, 2577.
- (37) Binet, L.; Fabre, J. M.; Montginoul, C.; Simonsen, K. B.; Becher, J. *J. Chem. Soc., Perkin Trans.* **1996**, *1*, 783.
- (38) Simonsen, K. B.; Svenstrup, N.; Lau, J.; Simonsen, O.; Mørk, P.; Kristensen, G. J.; Becher, J. *Synthesis* **1996**, 407.
- (39) Wudl, F.; Kruger, A. A.; Kaplan, M. L.; Hutton, R. S. *J. Org. Chem.* **1977**, *42*, 769.
- (40) (a) Narvor, N. L.; Robertson, N.; Weyland, T.; Killburn, J. D.; Underhill, A. E.; Webster, M.; Svenstrup, N.; Becker, J. *J. Chem. Soc., Chem. Commun.* **1996**, 1363. (b) Narvor, N. L.; Robertson, N.; Wallace, E.; Killburn, J. D.; Underhill, A. E.; Bartlett, P. N.; Webster, M. *J. Chem. Soc., Dalton Trans.* **1996**, 823.
- (41) (a) Kumasaki, M.; Tanaka, H.; Kobayashi, A. *J. Mater. Chem.* **1998**, *8*, 301. (b) Kobayashi, A.; Kumasaki, M.; Tanaka, H. *Synth. Met.* **1999**, *102*, 1768.
- (42) (a) Nakano, M.; Kuroda, A.; Maikawa, T.; Matsubayashi, G. *Mol. Cryst. Liq. Cryst.* **1996**, *284*, 301. (b) Ueda, K.; Goto, M.; Iwamatsu, M.; Sugimoto, T.; Endo, S.; Toyota, N.; Yamamoto, K.; Fujita, H. *J. Mater. Chem.* **1998**, *8*, 2195. (c) Misaki, Y.; Tani, Y.; Taniguchi, M.; Maitani, T.; Tanaka, K.; Bechgaard, K. *Mol. Cryst. Liq. Cryst.* **2000**, *343*, 59.
- (43) Rivera, N. M.; Engler, E. M. *J. Chem. Soc., Chem. Commun.* **1979**, 184.
- (44) Robertson, N.; Cronin, L. *Coord. Chem. Rev.* **2002**, *227*, 98.
- (45) (a) Valade, L.; Bousseau, M.; Gleizes, A.; Cassoux, P. *J. Chem. Soc., Chem. Commun.* **1983**, 110. (b) Valade, L.; Legros, J.-P.; Bousseau, M.; Cassoux, P.; Garbaskas, M.; Interrante, L. V. *J. Chem. Soc., Dalton Trans.* **1985**, 783.
- (46) The extended-Hückel molecular orbital calculations of [Ni-(tmdt)<sub>2</sub>] were performed by Y. Okano by the use of several parameter sets of atomic orbitals (e.g., the parameters reported by R. Hoffmann et al. (*J. Am. Chem. Soc.* **1976**, *98*, 1647; **1976**, *98*, 7240; **1979**, *101*, 592; **1987**, *109*, 118)). The calculated HOMO–LUMO gap  $\Delta E$  was scattered between 0.07 and 0.24 eV. Therefore, further calculations were made varying  $\Delta E$  by employing the following parameters of atomic orbitals: the valence shell ionization potential  $H_{ii}$ (eV) and the exponent  $\zeta_i$  of the Slater-type atomic orbital  $\chi_i$  are respectively (1) –20.0 and 1.817 for S 3s and –13.1 and 1.817 for S 3p or (2) –22.0 and 2.122 for S 3s, –10.5 and 1.827 for S 3p, –21.4 and 1.625 for C 2s, –11.4 and 1.625 for C 2p, –13.6 and 1.0 for H 1s, –10.95 and 2.1 for Ni 4s, –3.74 and 2.1 for Ni 4p, –9.19 and 2.190 for Pd 5s, and –5.30 and 2.150 for Pd 5p. The d orbitals of Ni and Pd are represented by a linear combination of two Slater-type orbitals:  $H_{ii}$ ,  $\zeta_i$ ,  $c_i$ , and  $c_{ii}$  values are –12.91, 5.98, 0.5264, 2.613, and 0.6372 for Pd 4d and –10.58, 5.75, 0.5681, 2.00, and 0.6294 for Ni 3d, respectively.
- (47) Rovira, C.; Novoa, J. J.; Mozos, J.; Ordejón, P.; Canadell, E. *Phys. Rev.* **2002**, *B65*, 081104(R).
- (48) Kobayashi, A.; et al. To be published.
- (49) Fujiwara, E.; Kobayashi, A.; Fujiwara, H.; Kobayashi, H. *Inorg. Chem.* **2004**, *43*, 1122.
- (50) Tamura, M.; Nakazawa, Y.; Shiomi, D.; Nozawa, K.; Hosokoshi, Y.; Ishikawa, M.; Takahashi, M.; Kinoshita, M. *Chem. Phys. Lett.* **1991**, *186*, 401.
- (51) Matsubayashi, G.; Takahashi, K.; Tanaka, T. *J. Chem. Soc., Dalton Trans.* **1988**, 967.
- (52) Kobayashi, A.; Fujiwara, E.; Suzuki, W.; Sasa, M.; Fujishiro, Y.; Nishibori, E.; Takata, M.; Sakata, M.; Okano, Y.; Fujiwara, H.; Kobayashi, H. *J. Phys. IV France* **2004**, *114*, 419.
- (53) Kariuki, B. M.; Serrano-González, H.; Johnston, R. L.; Harris, K. D. M. *Chem. Phys. Lett.* **1997**, *280*, 189.
- (54) (a) Takata, M.; Umeda, B.; Nishibori, E.; Sakata, M.; Saito, Y.; Ohno, M.; Shinohara, H. *Nature* **1995**, *377*, 46. (b) Takata, M.; Nishibori, E.; Sakata, M. *Z. Kristallogr.* **2001**, *216*, 71.
- (55) Belo, D.; Alves, H.; Lopes, E. B.; Duarte, M. T.; Gama, V.; Henriques, R. T.; Almeida, M.; Pérez-Benítez, A.; Rovira, C.; Veciana, J. *Chem. Eur. J.* **2001**, *7*, 511.
- (56) Schiødt, N. C.; Bjørnholm, T.; Bechgaard, K.; Neumeier, J. J.; Allgeier, C.; Jacobsen, C. S.; Thorup, N. *Phys. Rev. B* **1996**, *53*, 1773.
- (57) Schultz, A. J.; Wang, H. H.; Soderholm, L. C.; Sifter, T. L.; Williams, J. M.; Bechgaard, K.; Whangbo, M.-H. *Inorg. Chem.* **1987**, *26*, 3757.
- (58) Dautel, O. J.; Fourmigué, M. *Inorg. Chem.* **2001**, *40*, 2083.
- (59) Suzuki, W.; Fujiwara, E.; Kobayashi, A.; Fujishiro, Y.; Nishibori, E.; Takata, M.; Sakata, M.; Fujiwara, H.; Kobayashi, H. *J. Am. Chem. Soc.* **2003**, *125*, 1486.
- (60) The BE values of Au4f<sub>5/2</sub> and Au4f<sub>7/2</sub> of [Au(tmdt)<sub>2</sub>] are 90.3 and 86.7 eV, and those of (<sup>109</sup>Bu<sub>4</sub>N)[Au(tmdt)<sub>2</sub>] are 90.5 and 86.7 eV, respectively. (Kondo, H.; Ohta, T. Private communications.)
- (61) Ishibashi, S.; Terakura, K.; et al. To be published.
- (62) Kanoda, K.; et al. To be published.
- (63) Nishibori, E.; et al. To be published.
- (64) Suzuki, W.; Fujiwara, E.; Kobayashi, A.; Fujishiro, Y.; Nishibori, E.; Takata, M.; Sakata, M.; Okano, Y.; Kobayashi, H. *Chem. Lett.* **2003**, *32*, 1106.
- (65) Suzuki, W.; Fujiwara, E.; Kobayashi, A.; Hasegawa, A.; Miyamoto, T.; Kobayashi, H. *Chem. Lett.* **2002**, 936.
- (66) Kobayashi, A.; Sasa, M.; Suzuki, W.; Fujiwara, E.; Tanaka, H.; Tokumoto, M.; Okano, Y.; Fujiwara, H.; Kobayashi, H. *J. Am. Chem. Soc.* **2004**, *126*, 426.
- (67) Tsuda, A.; Osuka, A. *Science* **2001**, *293*, 79.
- (68) Tsuda, A.; Furuta, H.; Osuka, A. *Angew. Chem., Int. Ed.* **2000**, *39*, 2549.
- (69) Martin, R. E.; Diederich, F. *Angew. Chem., Int. Ed.* **1999**, *38*, 1350.
- (70) Tanaka, S.; Yamashita, Y. *Synth. Met.* **1997**, *84*, 229.
- (71) Takimiya, K.; Kato, K.; Aso, Y.; Ogura, F.; Otsubo, T. *Bull. Chem. Soc. Jpn.* **2002**, *75*, 1795.
- (72) Perepichka, D. F.; Bryce, M. R.; Batsanov, A. S.; McInnes, E. J. L.; Zhao, J. P.; Farley, R. D. *Chem. Eur. J.* **2002**, *8*, 4656.
- (73) Ishibashi, S.; et al. To be published.

CR030656L